ELSEVIER

Contents lists available at ScienceDirect

# Journal of Drug Delivery Science and Technology

journal homepage: www.elsevier.com/locate/jddst





# Intradermal delivery of nanohybrid thermosensitive hydrogels loaded with chondroitin sulphate coated pomegranate lipid carriers via hollow microneedles for effective rheumatoid arthritis management

Mariam Zewail<sup>a,\*</sup>, Haidy Abbas<sup>a</sup>, Nesrine El Sayed<sup>b</sup>, Nihal M. El Newehy<sup>c</sup>, Heba Abd-El-Azim<sup>a,d</sup>

- <sup>a</sup> Department of Pharmaceutics, Faculty of Pharmacy, Damanhour University, Damanhour, 22511, Egypt
- <sup>b</sup> Department of Pharmacology and Toxicology, Faculty of Pharmacy, Cairo University, Cairo, Egypt
- <sup>c</sup> Department of Pharmacognosy, Faculty of Pharmacy, Damanhour University, Damanhour, 22511, Egypt
- <sup>d</sup> Postdoc Brigham and Women's Hospital, Harvard Medical School, Harvard University, USA

#### ARTICLE INFO

#### Keywords: Autoimmune diseases Hollow microneedles Antigen-induced arthritis Stimulus-responsive hydrogels

#### ABSTRACT

Rheumatoid Arthritis (RA) is a common inflammatory arthritis type that significantly affects physical functions, leading to restrictions in daily activities. The current study aims to develop an effective nano-based drug delivery system for RA management using pomegranate peel extract (POM). POM was encapsulated in nanostructured lipid carriers (NLCs), coated with chondroitin sulphate (CHS) to actively target CD44 receptors that are over expressed in rheumatic joints. The optimized NLCs were loaded into Pluronic F127 hydrogels to prepare thermosensitive nanohybrid hydrogels for intradermal administration via AdminPenTM MNs hollow microneedles (Ho-MNs). The UPLC-ESI-MS/MS analysis of POM identified 76 compounds, predominantly polyphenols, known for anti-inflammatory and antioxidant properties. NLCs were prepared using the melt emulsification method, showing particle sizes ranging from 64.7  $\pm$  0.34 to 341  $\pm$  2.5 nm, zeta potentials between -17  $\pm$  1.34 mV and  $-30\pm0.98$  mV, and high entrapment efficiencies (96.34  $\pm$  0.34–98.89  $\pm$  0.12 %). Nanohybrid hydrogels extended the release period of POM from 6 days to 13 days and reduced burst effects. Ex vivo studies confirmed effective skin penetration by AdminPenTM MNs. In vivo studies in rats with AIA demonstrated that POM nanohybrid hydrogels significantly relieved joint swelling and reduced TNF- $\alpha$ , IL-1 $\beta$ , MDA, and MMP-3 levels, while increasing NRF2 level. Histopathological examination revealed that the nanohybrid hydrogel-treated group had normal joint and cartilage structure. This novel system offers a minimally invasive, sustained-release approach for RA treatment, enhancing bioavailability and the therapeutic efficacy of POM, thus providing a promising alternative to conventional therapies.

#### 1. Introduction

Arthritis is a broad word for a variety of inflammatory joint illnesses. Rheumatoid arthritis (RA) and osteoarthritis are the most frequent clinical disorders, affecting almost 4 % of the world's population and severely limiting mobility [1,2]. RA is a chronic inflammatory illness characterised by inflammation of joint tissues such as synovium and cartilage, causing joint discomfort, swelling, and deformity [2]. Based on the WHO's latest reports, about 18 million people suffer from RA worldwide. The age-standardized female-to-male prevalence ratio was 2.45, with a greater prevalence in females [3]. It is expected that by

2050, about 31.7 million individuals will be living with RA worldwide [4].

Despite the ideal use of today's antirheumatic agents, the majority of RA patients suffer from chronic pain and severe functional decline as these therapies are primarily effective in preventing joint inflammation and soft tissue swelling but ineffective in preventing cartilage breakdown and joint destruction [5] Besides the systemic toxicity associated with long-term drug distribution in non-targeted sites [6].

The use of medicinal plant remedies to treat chronic ailments, such as RA, is so widespread and growing [7]. Pomegranate (*Punica granatum* L.) POM is an ancient fruit-bearing shrub or small tree native to the

E-mail addresses: mariamzewail@gmail.com, mariamzewail@pharm.dmu.edu.eg (M. Zewail).

<sup>\*</sup> Corresponding author.

Middle East and South Asia [8]. The various fruit parts of POM have strong biological actions such as anti-inflammatory, anti-cancer, anti-oxidant anti-aging, anti-diabetic, hepatoprotective, and cardiovascular and the ability to prevent arthritis [9,10]. Pomegranate peel extract (PPE) has garnered significant interest because of its high concentration of polyphenols, especially ellagic acid and ellagitannins such as punicalagin, punicalin and pedunculagin, which makes it a promising natural ingredient for various therapeutic applications [11].

However, the medicinal application of natural products, including POM faces several physicochemical and biopharmaceutical challenges, such as low solubility and/or stability, poor bioavailability, rapid metabolism, short half-life, and significant plasma protein binding. These issues may be effectively tackled through nanoformulation strategies, which can potentially enhance the therapeutic efficacy of natural products [12].

Nanoencapsulation is one of the strategies to enhance the transdermal delivery of medications for RA management [13]. Nanohybrid hydrogel is a term used to describe hydrogels loaded with lipid nanocarriers, including nanostructured lipid carriers (NLCs). NLCs are lipid nanoparticles of the second generation consisting of solid lipid matrices combined with liquid lipids (oils). NLC's solid matrix allows them to firmly immobilise medicines and prevent particles from aggregating. The liquid oil droplets in the solid matrix boost drug loading capacity, whilst the less ordered lipid matrix provides for better drug accommodation [14,15]. The surface of NLCs has been modified with different polymers, like hyaluronic acid [16–18], chitosan [19] and chondroitin sulphate (CHS) [16,18,20]. CHS, a natural carbohydrate biopolymer, is a nutraceutical that helps prevent cartilage deterioration [21,22]. Moreover, CHS can target CD44 receptors that are overexpressed in inflamed rheumatic joints [16,18].

Besides, nanoencapsulation, micro-needles (MNs) stand out as a one of the methods for increasing cutaneous medication penetration. To prevent pain stimulation, MNs are physically made to efficiently pierce the stratum corneum without getting to the nerve endings [13]. Hollow microneedles (Ho-MNs) are one of the types of MNs which have microfluidic channels that disrupt the upper layers of the skin upon application, creating micro-conduits to deliver liquid medications. They have been translated to several commercially available products such as AdminPen<sup>TM</sup> Ho-MNs that are used in this study and can be mounted on any available standard syringe [23].

The current study's main objective is to prepare a drug delivery system that can provide effective RA management with minimum side effects by combining nanohybrid thermosensitive hydrogels and Ho-MNs to ensure effective, localized sustained drug delivery to the joint via the transdermal route. This was attained by preparing CHS-coated NLCs encapsulating POM, a herbal medicine with minimal side effects. The utilization of CHS as a coating polymer for NLCs would add additional value to NLCs, as CHS can actively target CD44 receptors that are overexpressed in inflamed joints, in addition to the innate joint healing properties of CHS. Moreover, oleic acid's anti-inflammatory and antioxidant effects are used in NLCs preparation. Then, the optimized formulation was loaded in Pluronic F127 thermosensitive hydrogels to act as a depot to prolong the release of POM from CHS-NLCs. Their efficacy was tested in rats with the AIA model after their application following intradermal injection using AdminPen™ Ho-MNs. This study is considered the first report of the preparation of Pluronic F127 nanohybrid hydrogels loaded with CHS-coated NLCs loaded with POM extract and injecting them using (Ho-MNs) in rats with the AIA model.

#### 2. Materials

Compritol 888 ATO, caproyl 90 and precirol were obtained from Gattefossé, (Saint-Priest, France). Pluronic F127 and stearic acid were kindly provided by Pharonia Pharmaceutical Companies (Alexandria, Egypt). Chondroitin sulphate (96 %) was provided by Pharco Pharmaceutical Company (Alexandria, Egypt). Oleic acid 98 % was bought from

Nice Chemicals (Kerala, India). The AdminPen<sup>TM</sup> device was purchased from NanoBioSciences LLC, USA. Rat ELISA kits were purchased from Cusabio Technology LL (Houston, USA). AdminPen<sup>TM</sup> metallic hollow microneedles were purchased from NanoBioSciences LLC, USA. All other chemicals and reagents were analytical grade.

#### 3. Methods

#### 3.1. Plant material and extraction

Samples of pomegranate fruits *Punica granatum* (L.), cultivar H-116, were provided by Nubaria farms for pomegranate in Al Beheira Governorate, Egypt in September 2023. Dr Tarek Elbolok, Department of Medicinal and Aromatic Plants, National Research Institute, Cairo performed taxonomic identification. Peels were separated, cleaned, airdried, ground by a blender, extracted with 70 % ethanol, and concentrated under vacuum (40 °C) by a rotary evaporator (Hei-VAP Value, Heidolph) to give a dry extract. The dried extract (PPE) was saved at  $-20\ ^{\circ}\text{C}$  until used.

#### 3.2. UPLC- Qqq -MS/MS analysis

The chemical profiling of PPE was conducted using UPLC-Qqq-MS/ MS through ESI-MS positive and negative ion acquisition mode according to a previously published method [24]. In brief, the sample was dissolved in HPLC-grade methanol (100  $\mu g/mL$ ) and filtered through a 0.2 µm membrane disc filter. A 10 µL injection volume was used. The UPLC system (Acquity, Waters®, Milford, MA, USA) was equipped with an Acquity UPLC-BEH C18 reversed-phase column (1.7 µm particle size,  $2.1\times50$  mm). The mobile phase flow rate was set to 0.2 ml/min, and a gradient elution program was used, consisting of acidified water (0.1 %formic acid) and acidified methanol (0.1 % formic acid), over a 35-min run. Mass spectrometric analysis was performed on a XEVO TQD triple quadrupole mass spectrometer (Waters Corporation, Milford, MA, USA) using ESI with the following parameters: 30 eV cone voltage, 3 kV capillary voltage, 150 °C source temperature, and 440 °C desolvation temperature, with vacuum provided by an Edwards® vacuum pump (Chandler, AZ, USA). Mass spectra were detected in the range of 50–1200 m/z using MassLynx 4.1 software, and peaks were tentatively identified by comparing their mass spectra and fragmentation patterns with previously reported data.

# 3.3. Preparation of NLCs and selection of the lipid phase

#### 3.3.1. Preliminary screening of solid lipid, liquid lipid and their miscibility

 $3.3.1.1.\,$  Screening of liquid lipids. By adding an excess of POM to 3 ml of oils in tiny vials, the saturation solubility of POM in various liquid lipids, such as oleic acid and capryol 90 was ascertained. After being securely sealed and constantly agitated at 100 rpm for 24 h at 25  $\pm$  2 °C in a shaking water bath, the vials were allowed to reach equilibrium for another 24 h. After 48 h, each saturated sample was centrifuged for 10 min at 5000 rpm. After the supernatant was removed and dissolved in ethanol, the UV spectrophotometer was used to measure the solubility of POM 385 nm [25].

3.3.1.2. Screening of solid lipids. Three solid lipids—stearic acid, Precirol® ATO 5, and Compritol® 888 ATO—were selected for screening based on their biocompatibility, widespread use in lipid-based nanocarriers, and differing fatty acid chain compositions, which influence solubility and encapsulation behavior. To assess the solubility of POM in each lipid, 100 mg of each lipid was weighed, melted, and maintained at a temperature 5–10°C above its melting point. POM was then incrementally added (1–2 mg per step) under constant stirring until the lipid became saturated. Solubilization was assessed visually, with complete

solubilization defined as the formation of a **clear**, **homogenous mixture with no visible crystals or phase separation**, consistent with previously reported protocols. The lipid exhibiting the **highest solubilization capacity** for POM under these conditions was selected for further formulation development [26–28].

3.3.1.3. Solid and liquid lipids' miscibility. Visual inspection was used to verify the miscibility of solid and liquid lipids before binary lipid phase selection. The drug's highest solubility was seen in the solid and liquid lipid mixtures that showed the best clarity, homogeneity, turbidity, and phase separation. In separate glass vials, solid lipids were melted with

assessed through centrifugal ultrafiltration utilizing a Centrisart-I tube with a molecular weight cutoff (MWCO) of 300 kDa, manufactured by Sartorius AG, Goettingen, Germany. The external tube of the Centrisart set contained two ml of the formula. The sample was subsequently subjected to centrifugation in a cooling centrifuge (Sigma 3-30 KS, Sigma Laborzentrifugen GmbH, Osterode, Germany) at 5000 rpm and 4 °C for 15 min. The supernatant was retained in the internal tube of the Centrisart. The concentration of POM in the supernatant was measured using UV spectroscopy at 385 nm [25].

The % EE was determined using the following equation:

$$EE~(\%) = \frac{Total~POM~concentration - concentration~of~unencapsulated~POM}{Total~POM~concentration}~x~100$$

liquid lipids (1:1). Additionally, the congealed bulk was inspected for homogeneity under a microscope. The lipid phase for the NLC design was chosen from among the mixtures that exhibit good miscibility, no signs of turbidity, and no phase separation [18].

# 3.3.2. Preparation of uncoated and chondroitin sulphate (CHS) coated

NLCs were prepared using the hot emulsification method previously reported by Zewail et al. [16,18]. A lipid phase composed of compritol (150 mg), 35 mg of oleic acid and POM (20 or 60 mg) was heated and kept at 85  $^{\circ}$ C. An aqueous phase composed of 0.2  $^{\circ}$ C Tween 80 was heated to the same temperature. Hot aqueous was added to the lipid phase and ultrasonication (SONOPULS MINI20 probe tip sonicator, BANDELIN electronic GmbH & Co., Germany) was carried out at 60  $^{\circ}$ C amplitude for 5 min. The formed pre-emulsion was added to an external aqueous phase containing 0.5  $^{\circ}$ C CHS, then the produced emulsion was sonicated for a second time using the aforementioned conditions.

To prepare uncoated NLCs, the same procedure was followed with the exception that the secondary aqueous phase was composed of distilled water instead of CHS.

# 3.4. Preparation of plain and POM pluronic F127 thermosensitive nanohybrid hydrogels

To prepare plain F127 hydrogels  $2\ g$  of Pluronic F127 was dissolved in 10 ml of distilled water in an ice bath using a magnetic stirrer for  $1\ h$ .

**To prepare POM-loaded F127 hydrogels**, 2 g of F127 was mixed with either POM-loaded CHS-coated NLCs (POM-CHS-NLCs) or POM suspension in an ice bath under magnetic stirring for 1 h. The resultant hydrogels were stored in the refrigerator till further investigations [16, 29,30].

# 3.5. Characterization of POM-NLCs

# 3.5.1. Particle size, polydispersity index (PDI) and zeta potential measurements

Measurements of particle size, PDI, and zeta potential were conducted utilizing the Nanotrac/Wave II/Q/Zeta from Microtrac MRB (VERDER SCIENTIFIC GmbH & Co. KG, Haan, Germany). Before measurement, 1 ml samples were diluted with deionized water at a ratio of 1:10, at a scattering angle of 173° and all measurements were performed at room temperature (RT) in triplicates and reported as mean  $\pm$  standard deviation (SD).

## 3.5.2. Measurement of entrapment efficiency (EE%)

The encapsulation efficiency of POM incorporated into NLCs was

#### 3.5.3. Morphological examination

The morphology of the selected formulation was examined using a transmission electron microscope (TEM, JEM-100CX; JEOL, Japan). After diluting with distilled water at a 1:20 ratio and sonication for 5 min, a droplet of the diluted dispersion was placed onto a 300-mesh carbon-coated copper grid, followed by staining with a droplet of uranyl acetate. The solution was allowed to settle for 5 min to ensure proper adhesion, after which excess solution was removed using filter paper. The grids were permitted to air dry before microscopic examination [31].

# 3.6. Characterization of plain and POM-loaded 127 nanohybrid thermosensitive hydrogels

# 3.6.1. Determination of gelation time

The gelation time of both plain and POM-loaded hydrogels was assessed at temperatures of 25 and 37  $^{\circ}\text{C}$  utilizing the test tube inversion method. Hydrogel samples (1 ml in Wizerman tubes) were incubated in a water bath at the specified temperatures and assessed every 20 s by tilting the tubes. The cessation of the sample flow was recorded. Measurements were conducted in triplicate and results represented as mean + SD

#### 3.6.2. Thermal reversibility

After gelation at 37 °C, hydrogels were cooled to 4 °C to test their thermal reversibility. Thermo-reversible hydrogels convert to liquids at 4 °C, whereas thermo-irreversible hydrogels remain in the gel form at 4 °C. Measurements were carried out in triplicates and results represented as mean  $\pm$  SD.

#### 3.6.3. pH

The pH of plain and POM-loaded hydrogels, either with free form or POM-CHS-NLCs was evaluated using a pH meter (Model 3510, Midwest Scientific, Saint Louis) at RT (n=3).

# 3.6.4. Injectability

The injectability of plain and POM-loaded hydrogels, either with free form or POM-CHS-NLCs was tested as previously described [16,30, 32–35]. In summary, 3 ml of hydrogel was placed in a glass syringe with a 27-gauge needle. Syringes were kept at room temperature for at least 10 min before being used to determine injection timings. The injection time was calculated by vertically attaching a 1-kg mass to the top of the plunger and monitoring how long it took to discharge 1 ml of sample from the syringe. All measurements were done in triplicates.

#### 3.6.5. Measurement of hydrogel viscosity

The viscosity of plain and POM-loaded hydrogels either with free form or POM-CHS-NLCs was determined at 100 rpm at RT by a Cone and Plate Brookfield Viscometer with an S-52 spindle (Brookfield DV II-RV, USA). Measurements were conducted three times for a 1 ml hydrogel sample and results are represented as mean  $\pm$  SD.

#### 3.6.6. In vitro drug release

The *in vitro* release study was conducted for POM suspension, free POM in F127 hydrogel and selected POM-NLCs either in free form or loaded in F127 hydrogel using dialysis technique (Visking®, MWCO 12,000–14,000; SERVA, Heidelberg, Germany). The bags were placed in 100 ml of PBS, pH 7.4 in a shaking water bath (Wisebath®, London, UK) at 100 rpm and 37 °C to ensure sink conditions [36]. Samples of the release media were withdrawn at predefined time intervals, and the amount of POM released was quantified spectrophotometrically at 385 nm [25]. During the sampling period, the removed medium was replaced by a fresh buffer. Each experiment included three replicates.

# 3.7. Ex vivo insertion study to evaluate skin penetration of hollow microneedles-assisted delivery of POM- NLCs in F127 nanohybrid hydrogels

The AdminPen<sup>TM</sup> array consisted of 43 stainless-steel MN shafts of 1200 µm height. The quality of skin penetration utilizing AdminPen™ Ho-MNs was assessed as previously reported, with appropriate adjustments [13,37,38]. Full-thickness human skin was preserved and obtained following abdominal plastic surgery performed on a male volunteer. After removing subcutaneous fats, the upper skin surface was rinsed with normal saline solution, dried, carefully covered and preserved at -20 °C for future use. This protocol adhered to the previously established optimized conditions for the preservation of human skin for 3-6 months. An AdminPen<sup>TM</sup>, featuring a 43 stainless steel metallic Ho-MNs array with a length of 1200 µm, was utilized for the intradermal injection of both free POM on F127 hydrogel and POM-CHS-NLCs in F127 hydrogel into the cleansed skin's exterior surface, employing the thumb and index finger technique and digital photographs of the skin were captured after the MNs were removed using a Samsung Galaxy S23 Ultra, dual pixel, 12 MP, PDAF. The number of optically clear pores created by Ho-MNs was determined, and then the percentage of percutaneous penetration was calculated using the following equation:

 $\label{eq:Thepercentage} The \ percentage \ of \ penetration = \frac{\textit{Number of created holes in skin}}{\textit{Total number of hollow microneedles}} \\ \times 100$ 

#### 3.8. In vivo study

#### Ethical approval

The Institutional Animal Care and Use Committee (IACUC) of the Faculty of Veterinary Medicine at Cairo University approved this experimental protocol, and assigned ethical approval number PT (3461) in 2023.

#### 3.8.1. Experimental design and RA induction

Adult male Sprague Dawley rats (180  $\pm$  20 g) were housed in a temperature-controlled environment (25  $\pm$  0.5 °C) with unrestricted access to a standard pellet diet and water, following a 12-h light/dark cycle. Twenty male rats were allocated into four groups, each consisting of five individuals (n = 5). RA induction was performed following the methodology established by our research group in prior publications [13,17,39,40]. RA was induced through a single injection of 0.2 ml of complete Freund's adjuvant (CFA) into the right knee joints of rats, with the left knee joints acting as controls.

Fig. 1 illustrates the various experimental groups. Groups 3 and 4 received two 200  $\mu l$  intradermal injections of Ho-MNs in the right knee joints on days 4 and 9 of the experiment, administering a POM dose of 25 mg/kg [41]. Following 14 days, rats were anaesthetized and euthanized via cervical dislocation under thiopental anaesthesia (50 mg/kg) [42]. The joints were subsequently dissected and preserved in a 10 % formalin solution. Blood samples were collected and centrifuged at 5000 rpm at room temperature for 15 min. The serum was subsequently frozen at  $-80\ ^{\circ}\text{C}$  for future analysis.

#### 3.8.2. Joint diameter assessment

To study the effect of various treatments on rat knee joint oedema, the anteroposterior diameters of the rat knees were measured using a digital micrometer at predetermined time intervals (days 0, 4, 7, and 14)

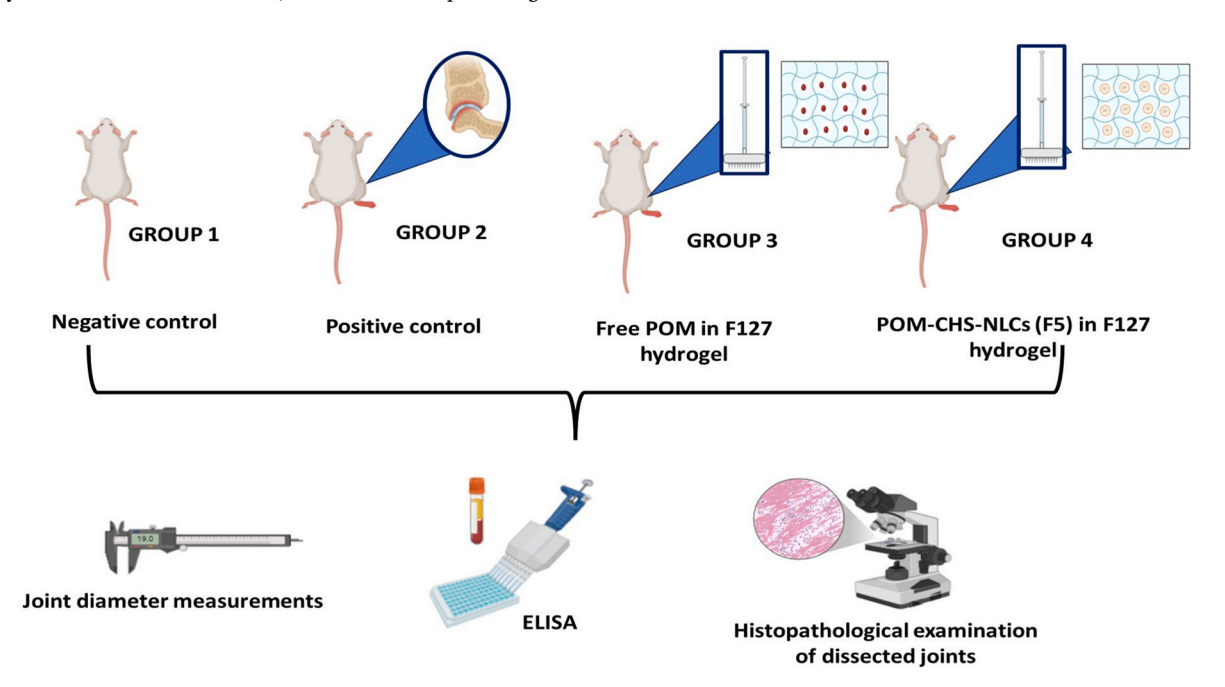


Fig. 1. Schematic representation illustrating the different in vivo experimental groups and further characterization techniques.

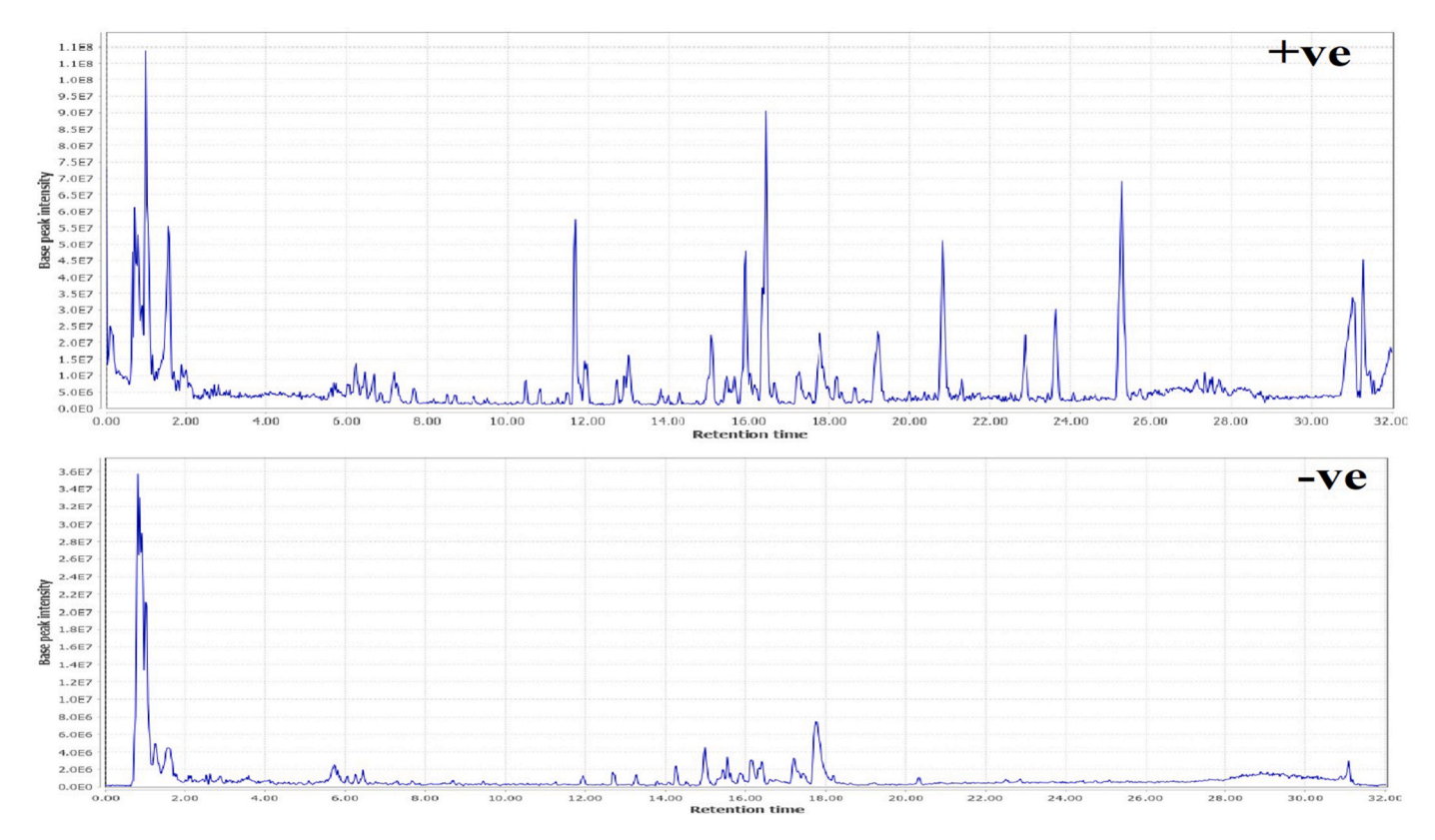


Fig. 2. Base Peak Chromatograms (BPC) collected in the negative and positive modes for PPE.

#### 3.8.3. Enzyme-linked immunosorbent assay (ELISA)

At the end of the experiment, rats were sedated and blood samples were obtained. Levels of tumour necrosis factor  $\alpha$  (TNF- $\alpha$ ), interleukin 1 $\beta$  (IL1 $\beta$ ), malondialdehyde (MDA), matrix metalloproteinases (MMP3) (My BioSource, San Deigo, CA, USA) and nuclear respiratory factor 2 (NRF2) (Cusabio Technology LL, Houston, USA) were assessed using ELISA kits according to the manufacturer instructions.

# 3.8.4. Histopathological study

At the end of the experiment, animals were sacrificed, and samples of the knee joints were collected. All samples were subjected to a two-week decalcification process following fixation in 10 % formalin. After decalcification, the samples were subjected to standard processing, embedding, sectioning, and subsequent staining with hematoxylin and eosin (H&E) [43]. Histopathological examination was conducted utilizing an electric light microscope (Olympus BX50, Tokyo, Japan) linked to a DP27 digital camera (Olympus) for the acquisition of photomicrographs.

## 3.9. Statistical analysis

Results are presented as the mean  $\pm$  standard deviation (SD). Statistical analyses were conducted using Prism 9 software. NLCs particle size and zeta potential were analyzed using the student t-test (p < 0.05), while ELISA results were assessed with One-way ANOVA (P < 0.0001).

# 4. Results and discussion

# 4.1. Metabolite profiling via UPLC-ESI-MS/MS

Pomegranate peel is the tough outer layer of the fruit, along with the inedible film inside, discarded as industrial waste, which is not only a waste of resources but also pollutes the environment [24].

UPLC-ESI-MS/MS analysis of PPE was performed to reveal its

phytochemical constituents. Fig. 1 represents the base peak chromatogram in the positive and negative ion modes. 76 compounds, mainly flavonoid glycosides, tannins, phenolic acids and alkaloids, have been tentatively identified by comparing their MS characteristics and fragmentation pattern with in-house and online comprehensive databases and previously reported literature data on PPE (Table 1). Polyphenols demonstrated the predominant class of metabolites identified in PPE. In particular, ellagic acid, punicalagins, granatin A, quercetin, kaempferol and anthocyanins exert their effects by reducing inflammation, oxidative stress, and joint degradation, all of which are key contributors to arthritis [44-46]. These compounds have been shown to reduce inflammation through downregulation of the expression levels of pro-inflammatory cytokines such as IL-6, IL-5, IL-8, IL-10, IL-1β, IL-18, TNF-α, and IFN-γ, as well as the concentrations of COX, NF-κB, MPO, NO, and MMPs [47]. Gallic acid along with ellagic acid, has been reported to have anti-inflammatory and antioxidant effects. They can help reduce oxidative stress and inflammatory responses, making them potentially beneficial in managing inflammatory joint diseases like arthritis [48,49]. Punicalagins can inhibit the production of inflammatory mediators like nitric oxide (NO) and prostaglandins, which play key roles in the pathogenesis of arthritis. They also have a protective effect on joints and may help reduce cartilage degradation [50]. Triterpenoids (e.g., betulonic acid) found in pomegranate peel have been investigated for their potential anti-arthritic properties [51]. These compounds are known to inhibit the production of pro-inflammatory cytokines and enzymes such as COX-2, helping to reduce pain and swelling associated with conditions like RA [51]. This powerful bioactive composition encourages us to investigate PPE's in vitro anti-arthritic activity and enhance this therapeutic efficacy through nanoformulation strategies.

#### 4.2. Lipid phase selection

A lipid screening is a simple but important step in NLCs formulation, due to the effect of drug solubility on the entrapment and encapsulation

 Table 1

 Metabolites identified in *Punica granatum* samples extracts using UPLC-MS in positive and negative ionization modes.

No.	Rt (min.)	Identified compounds	Precursor ion	Chemical classes	Elemental composition	$MS^n$ ions $m/z$ (–)
1.1	0.66	Mannitol <sup>a</sup>	181.1 (M – H)	Sugar alcohol	C6H14O6	163, 149, 131, 119
2.2	0.88	Quinic acid <sup>a</sup>	191.1 (M − H) <sup>-</sup>	Organic acids	C7H12O6	111,129
.3	1.01	Fragment of quinic acid	$131.1 (M + H)^{+}$	Organic acids	C6H10O3	129
.4	1.15	Quinic acid methyl ester	205 (M-H)-	Organic acids	C8H14O6	111, 129
.6	1.19	cyanidin diglycoside	$611.3 (M + H)^{+}$	Anthocyanins	C27H31O16	164, 261, 289, 367
.7	1.34	Punicalagin α	1083.4 (M – H)	Tannin	C48H28O30	781, 721, 601, 299
.8	1.35	Pyrogallol <sup>a</sup>	$127.1 (M + H)^{+}$	Tannin	C6H6O3	97
.9	1.36	Caffeic acid <sup>a</sup>	179.2 (M – H)	Phenolic acids	C9H8O4	135
.10	1.38	Vanillic acid hexoside	329.2 (M – H)	Phenolic acids	C8H8O4	269, 209, 181
0.11	1.49	Secoisolariciresinol	363.2 (M + H) <sup>+</sup>	Lignans	C20H26O6	165, 179, 331, 313, 346
1.12	1.75			Tannin	C48H28O30	781, 721, 601, 299
	1.73	Punicalagin β	1083.4 (M – H)		C34H26O22	
2.13		Digalloyl-HHDP-hex (pedunculagin II)	785.2 (M – H) <sup>+</sup>	Tannin		685, 633, 483, 301
3.14	1.9	Ellagic acid deoxy hexose	449.1 (M + H) <sup>+</sup>	Tannin	C20H16O12	299
4.15	1.97	Pedunicalagin I Bis-HHDP-hex	783.1 (M – H)	Tannin	C34H24O22	765, 481, 301, 275
5.16	2.04	Cyanidin-3-glucoside <sup>a</sup>	$449.2 (M + H)^{+}$	Anthocyanins	C21H20O11	301, 151
6.17	2.1	Punigluconin	$801.3 (M - H)^{-}$	Tannin	C34H26O23	781, 649, 499, 347, 301
7.18	2.23	Casuarictin	$935.2 (M - H)^{-}$	Tannin	C39H35O27	783, 633,301
8.19	2.3	Fertaric acid	$325.3 (M - H)^{-}$	Phenolic acids	C14H14O9	193, 149
9.20	2.33	Granatin A ellagic acid derivative	799.3 (M – H)	Tannin	C34H24O23	781, 301, 273
0.21	2.63	Ellagitannin <sup>a</sup>	643.2 (M – H)	Tannin	C25H24O20	481
1.22	2.44	Granatin A	784.2 (M – H)	Tannin	C34H24O22	781, 479, 301, 273, 257
2.23	2.6	Malic acid <sup>a</sup>	179.2 (M + HCOO-	Organic acids	C4H6O5	115
			H)	. 0		-
3.24	2.71	Ferulic acid glucoside	355.2 (M – H)	Phenolic acids	C16H20O9	175, 160
4.25	2.81	Valoneic acid bilactone C-glucoside	643.2 (M – H)	Tannin	C27H16O19	571, 541, 511, 469, 451, 42
		9				
5.26	3.11	Ellagic acid glucoside	463.1 (M – H)	Tannin	C20H16O13	445, 403, 373, 343, 313, 30
6.27	3.14	Ferulic acid <sup>a</sup>	217.2 (M + Na) <sup>+</sup>	Phenolic acids	C10H10O4	101, 111, 113, 133, 161, 179
7.28	3.44	Emodin-8-glucoside	431.3 (M – H) <sup>-</sup>	Anthraquinone glycoside	C21H20O10	269
8.29	3.52	Atractylenolide I	$231.2 (M + H)^{+}$	Sesquiterpenoid lactone	C15H18O2	217, 122
9.30	3.85	Pelletierine <sup>a</sup>	$142.21 (M + H)^{+}$	Alkaloids	C8H15NO	139
0.31	4.04	Procyanidin dimer	$579.2 (M + H)^+$	Flavanol	C30H26O12	113, 175, 289, 341, 407, 425, 451
1.32	5.58	Ellagic acid pentoside	433.1 (M – H)	Tannin	C19H14O12	301
2.33	5.74	Quercetin 3-O-glucuronide	$475.3 (M - H)^{-}$	Flavonol glucuronide	C21H18O13	111, 161, 301
3.34	5.8	Galloyl-HDDP-glucuronide Lagerstannin C	651.4 (M + H) <sup>+</sup>	Tannin	C27H22O19	605, 497, 361, 301
4.35	5.81	Ellagic acid <sup>a</sup>	301.1 (M – H)	Tannin	C14H6O8	229, 185
5.36	6.04	Luteolin-glucoside	$449.2 (M + H)^{+}$	Flavone glycoside	C21H20O11	285, 271, 217
6.37	7.17	Luteolin-arabinoside	$419.2 (M + H)^{+}$	Flavone glycoside	C20H18O10	285, 199, 175
7.38	9.08	Liquiritin <sup>a</sup>	419.1 (M + H) <sup>+</sup>	Flavanone glycoside	C21H22O9	401, 257, 137, 119
8.39	9.44	Palmatine	$353.3 (M + H)^+$	Alkaloids	C21H22NO4	336, 322, 308, 294
9.40	10.75		753.2 (M + H) <sup>+</sup>		C35H44O18	
		(epi) gallocatechin-cyanidin-3-glucoside		Anthocyanins		591, 573, 423
0.41	11.06	Hydroxybenzoic acid glucoside	300.3 (M + H) <sup>+</sup>	Phenolic acids	$C_{13}H_{16}O_{8}$	179, 168, 137, 136,124
1.47	12.92	flavogallol	$453.2 (M + H)^+$	Tannin	C21H8O12	170
2.48	12.95	Quercetin-3-O-glucoside <sup>a</sup>	463.1 (M – H)	Flavonol glycoside	C21H20O12	265, 301
3.50	13.23	Catechin-gallocatechin	592.4 (M – H) <sup>-</sup>	Flavanol	C31H29O12	423, 305, 285, 179, 149, 13 125
4.51	13.36	Berberine <sup>a</sup>	$337.2 (M + H)^{+}$	Alkaloids	C20H18NO4	320, 306, 292, 278
5.53	13.82	p-Coumaroylquinic acid	337.4 (M - H)	Phenolic acids	C16H18O8	191, 163
5.56	14	p-coumaric acid glucoside	327.2 (M + H)+	Phenolic acids	$C_{15}H_{18}O_{8}$	276, 145, 117
7.57	14.03	Astilbin	449.3 (M – H)	Flavanone glycoside	$C_{21}H_{22}O_{11}$	303, 287, 153
8.60	14.88	Coumaric acid <sup>a</sup>	163.1 (M – H)	Phenolic acids	C9H8O3	147, 119
9.61	14.97	Phlorizin <sup>a</sup>	$437.4 (M - H)^{+}$	Bicyclic flavonoid	C21H24O10	297, 273, 167
0.64	15.22	(epi) gallocatechin-pelargonidin-3- hexoside	$737.2 (M + H)^{+}$	Anthocyanins	C36H33O17	575, 449, 407
	16.14	Myricetin 3-O-glucoside <sup>a</sup>	491 4 (M + LD+	Flavonol glycoside	C21H20O12	112 262 217 261 441
1	16.14	,	481.4 (M + H) <sup>+</sup>	0.0	C21H20O13	113, 262, 317, 361, 441
	16 15	Hyperoside <sup>a</sup>	$433.4 (M - H)^{-}$	Flavonol glycoside	C21H20O12	301, 300, 272, 229, 169, 12
2.70	16.15	Dalaman di din Oralina (11	400 4 (34 ****	Anthocyanins	C21H21O10	271
2.70 3.72	16.43	Pelargonidin-3-glucoside	432.4 (M – H)	* *		
2.70 3.72 4.74	16.43 16.65	Isolariciresinol	$361.2 (M + H)^{+}$	Lignans	C20H24O6	344, 345, 313
2.70 3.72 4.74 5.75	16.43 16.65 16.85	Isolariciresinol 5-O-Caffeoylquinic acid <sup>a</sup>	361.2 (M + H) <sup>+</sup> 353.3 (M - H) <sup>-</sup>	Phenolic acids	C16H18O9	191, 179
2.70 3.72 4.74 5.75 6.76	16.43 16.65 16.85 16.98	Isolariciresinol 5-O-Caffeoylquinic acid <sup>a</sup> Gallic acid <sup>a</sup>	$361.2 (M + H)^{+}$ $353.3 (M - H)^{-}$ $171.2 (M + H)^{+}$	Phenolic acids Phenolic acids	C16H18O9 C7H6O5	191, 179 125
2.70 3.72 4.74 5.75 6.76 7.77	16.43 16.65 16.85 16.98 17.07	Isolariciresinol 5-O-Caffeoylquinic acid <sup>a</sup> Gallic acid <sup>a</sup> Brevifolincarboxylic acid	361.2 (M + H) <sup>+</sup> 353.3 (M - H) <sup>-</sup> 171.2 (M + H) <sup>+</sup> 293.2 (M + H) <sup>+</sup>	Phenolic acids Phenolic acids Tannin	C16H18O9 C7H6O5 C13H8O8	191, 179 125 247
2.70 3.72 4.74 5.75 6.76 7.77	16.43 16.65 16.85 16.98	Isolariciresinol 5-O-Caffeoylquinic acid <sup>a</sup> Gallic acid <sup>a</sup>	$361.2 (M + H)^{+}$ $353.3 (M - H)^{-}$ $171.2 (M + H)^{+}$	Phenolic acids Phenolic acids	C16H18O9 C7H6O5	191, 179 125
2.70 3.72 4.74 5.75 5.76 7.77 3.79	16.43 16.65 16.85 16.98 17.07	Isolariciresinol 5-O-Caffeoylquinic acid <sup>a</sup> Gallic acid <sup>a</sup> Brevifolincarboxylic acid	361.2 (M + H) <sup>+</sup> 353.3 (M - H) <sup>-</sup> 171.2 (M + H) <sup>+</sup> 293.2 (M + H) <sup>+</sup>	Phenolic acids Phenolic acids Tannin	C16H18O9 C7H6O5 C13H8O8	191, 179 125 247
2.70 3.72 4.74 5.75 6.76 7.77 3.79 9.80	16.43 16.65 16.85 16.98 17.07 17.77	Isolariciresinol 5-O-Caffeoylquinic acid <sup>a</sup> Gallic acid <sup>a</sup> Brevifolincarboxylic acid Glycerol tri-octadecanic acid	361.2 (M + H) <sup>+</sup> 353.3 (M - H) <sup>-</sup> 171.2 (M + H) <sup>+</sup> 293.2 (M + H) <sup>+</sup> 871.9 (M - H) <sup>-</sup>	Phenolic acids Phenolic acids Tannin Acid	C16H18O9 C7H6O5 C13H8O8 C57H92O6	191, 179 125 247 784, 757, 681, 664
2.70 3.72 4.74 5.75 6.76 7.77 8.79 9.80 0.81	16.43 16.65 16.85 16.98 17.07 17.77 18.29	Isolariciresinol 5-O-Caffeoylquinic acid <sup>a</sup> Gallic acid <sup>a</sup> Brevifolincarboxylic acid Glycerol tri-octadecanic acid Quercetin <sup>a</sup> Pelargonidin-3-pentoside Galloyl-gallagyl-hexoside (pedunculagin	361.2 (M + H) <sup>+</sup> 353.3 (M - H) 171.2 (M + H) <sup>+</sup> 293.2 (M + H) <sup>+</sup> 871.9 (M - H) 303.4 (M + H) <sup>+</sup>	Phenolic acids Phenolic acids Tannin Acid Flavonol	C16H18O9 C7H6O5 C13H8O8 C57H92O6 C15H10O7	191, 179 125 247 784, 757, 681, 664 273, 257, 151, 135
2.70 3.72 4.74 5.75 5.76 7.77 3.79 9.80 0.81 1.82	16.43 16.65 16.85 16.98 17.07 17.77 18.29 18.37 19.15	Isolariciresinol 5-O-Caffeoylquinic acid <sup>a</sup> Gallic acid <sup>a</sup> Brevifolincarboxylic acid Glycerol tri-octadecanic acid Quercetin <sup>a</sup> Pelargonidin-3-pentoside Galloyl-gallagyl-hexoside (pedunculagin III)	361.2 (M + H) <sup>+</sup> 353.3 (M - H) 171.2 (M + H) <sup>+</sup> 293.2 (M + H) <sup>+</sup> 871.9 (M - H) <sup>-</sup> 303.4 (M + H) <sup>+</sup> 403.1 (M + H) <sup>+</sup> 933.2 (M - H) <sup>-</sup>	Phenolic acids Phenolic acids Tannin Acid Flavonol Anthocyanins Tannin	C16H18O9 C7H6O5 C13H8O8 C57H92O6 C15H10O7 C20H18O9 C <sub>41</sub> H <sub>26</sub> O <sub>26</sub>	191, 179 125 247 784, 757, 681, 664 273, 257, 151, 135 271 915, 781, 721, 601
2.70 3.72 4.74 5.75 6.76 7.77 3.79 9.80 0.81 1.82	16.43 16.65 16.85 16.98 17.07 17.77 18.29 18.37 19.15	Isolariciresinol 5-O-Caffeoylquinic acid <sup>a</sup> Gallic acid <sup>a</sup> Brevifolincarboxylic acid Glycerol tri-octadecanic acid Quercetin <sup>a</sup> Pelargonidin-3-pentoside Galloyl-gallagyl-hexoside (pedunculagin III) 3-O-Caffeoylquinic acid <sup>a</sup>	361.2 (M + H) <sup>+</sup> 353.3 (M - H) <sup>-</sup> 171.2 (M + H) <sup>+</sup> 293.2 (M + H) <sup>+</sup> 871.9 (M - H) <sup>-</sup> 303.4 (M + H) <sup>+</sup> 403.1 (M + H) <sup>+</sup> 933.2 (M - H) <sup>-</sup> 353.4 (M - H) <sup>-</sup>	Phenolic acids Phenolic acids Tannin Acid Flavonol Anthocyanins Tannin	C16H18O9 C7H6O5 C13H8O8 C57H92O6 C15H10O7 C20H18O9 C <sub>41</sub> H <sub>26</sub> O <sub>26</sub> C16H18O9	191, 179 125 247 784, 757, 681, 664 273, 257, 151, 135 271 915, 781, 721, 601
1. 2.70 3.72 4.74 5.75 6.76 7.77 8.79 9.80 0.81 1.82 2.84 3.85 4.86	16.43 16.65 16.85 16.98 17.07 17.77 18.29 18.37 19.15	Isolariciresinol 5-O-Caffeoylquinic acid <sup>a</sup> Gallic acid <sup>a</sup> Brevifolincarboxylic acid Glycerol tri-octadecanic acid Quercetin <sup>a</sup> Pelargonidin-3-pentoside Galloyl-gallagyl-hexoside (pedunculagin III)	361.2 (M + H) <sup>+</sup> 353.3 (M - H) 171.2 (M + H) <sup>+</sup> 293.2 (M + H) <sup>+</sup> 871.9 (M - H) <sup>-</sup> 303.4 (M + H) <sup>+</sup> 403.1 (M + H) <sup>+</sup> 933.2 (M - H) <sup>-</sup>	Phenolic acids Phenolic acids Tannin Acid Flavonol Anthocyanins Tannin	C16H18O9 C7H6O5 C13H8O8 C57H92O6 C15H10O7 C20H18O9 C <sub>41</sub> H <sub>26</sub> O <sub>26</sub>	191, 179 125 247 784, 757, 681, 664 273, 257, 151, 135 271 915, 781, 721, 601

(continued on next page)

Table 1 (continued)

No.	Rt (min.)	Identified compounds	Precursor ion	Chemical classes	Elemental composition	$MS^n$ ions $m/z$ (–)
66.91	22.35	Genistin <sup>a</sup>	433 (M + H) <sup>+</sup>	Isoflavone glycoside	C21H20O10	271, 181
67.92	23.09	Myrcetin <sup>a</sup>	$319.4 (M + H)^{+}$	Flavonol	C15H10O8	113, 161, 219, 262
68.93	24.57	Punicalin (gallagyl-hexoside)	$783.1 (M + H)^{+}$	Tannin	C34H22O22	721, 601, 299
69.94	25.22	Glucogallin	$333.2 (M + H)^{+}$	Tannin	C13H16O10	125, 169
70.97	26.15	Hexahydroxydiphenic hexoside (HHDP)	483.2 (M + H)+	Tannin	C14H10O10	465, 423, 303, 277, 193
71.	25.58	Phylligenin	371.1 (M - H)	Lignans	C21-H24-O6	136
72.	26.84	Cosmosiin	$433.2 (M + H)^{+}$	Flavone	C21H20O10	269, 268
73.102	26.93	Phloretin <sup>a</sup>	$275.1 (M + H)^{+}$	Dihydrochalcone	C15H14O5	169, 127
74.104	27.52	Granatumol	$397.6 (M + H)^+$	Tannin	C24H44O4	381, 367, 284, 280, 264, 257, 249
75.106	27.77	Betulonic acid	$455.2 (M + H)^{+}$	Triterpenoid	C30H46O3	409, 205, 177, 119
76.107	28.48	Gallagic acid	639.4 $(M + H)^+$	Tannin	$C_{28}H_{14}O_{18}$	299, 271

<sup>&</sup>lt;sup>a</sup> Compound identified using reference standard.

efficiency of the system [52]. Liquid lipid screening demonstrated that POM showed the highest solubility in oleic acid (8 mg/ml), followed by capyrol 90 (4 mg/ml). On the other hand, POM solubility in stearic acid, compritol, and precirol was 25, 42 and 40 mg/100 mg lipid, respectively. Different solid and liquid lipids showed good miscibility by visual observations. Also, congealed masses of different binary mixtures showed good uniformity during microscopic examination. Based on these findings, compritol and oleic acid were used to prepare NLCs as POM exhibited the highest solubility in them.

Compritol as a solid lipid possesses complex structure and less exact orientation, which allows higher drug loading. Compritol consists mainly of **glyceryl behenate**, a mixture of mono-, di-, and triglycerides of behenic acid. Its **long alkyl chains** and **amorphous nature** offer enhanced **drug entrapment** via interchain intercalation and reduce drug expulsion during storage. The **complex lipid matrix** also contributes to sustained release characteristics, which is beneficial for transdermal delivery applications.

Oleic acid was selected as the liquid lipid due to both its high solubility capacity for POM and its well-documented role as a skin penetration enhancer [53]. It disrupts the lipid packing in the stratum corneum, thereby enhancing percutaneous absorption. In addition, oleic acid exhibits antioxidant and anti-inflammatory properties, which may help reduce local irritation and support skin compatibility [54].

The combination of Compritol and oleic acid was thus selected to maximize drug loading, promote transdermal penetration, and improve formulation stability.

#### 4.3. Colloidal characteristics of POM-NLCs

We explored developing lipid nanocarriers since POM extract is

lipophilic. Various NLCs were created using the melt emulsification process. This approach is better than the solvent diffusion method since it avoids the utilization of organic solvents [18,55]. POM lipid carriers have been previously reported by Badawi et al. who prepared POM-loaded solid lipid nanoparticles using Plackett–Burman design and optimized formulation characteristics [36]. Also, Soleimanian et al. prepared POM-loaded NLCs using POM seed oil, beeswax and propolis wax but they did not use PPE or test the application of the prepared formulations [56].

CHS was chosen to modify the surface of NLCs to actively target RA-inflamed joints [16]. CHS is also claimed to have significant anti-inflammatory properties by decreasing the concentrations of many pro-inflammatory agents. Moreover, CHS has disease-modifying capabilities and is therefore classified as SYSADOA (Symptomatic slow-acting medication for Osteoarthritis) by the European League Against Rheumatism [21]. The schematic structure of CHS-NLCs is illustrated in Fig. 3 A.

The particle size of different formulations ranged from 64.7  $\pm$  0.34 nm to 341  $\pm$  2.5 nm (Table 2). It has previously been observed that gaps of up to 700 nm exist between interendothelial cell connections in rheumatic joints [17]. As a result, the particle size of the produced nanocarriers is appropriate for both passive targeting of rheumatic joints via increased permeation and retention (EPR) and active targeting via CHS coating [16,18,57]. Loading NLCs with POM resulted in increasing their particle size. The particle size of F1 (blank) and F2 (loaded with 20 mg POM) increased from 64.7  $\pm$  0.34 nm to 163.9  $\pm$  1.2 nm. Upon coating F2 with CHS, the particle size of the resultant formulation significantly increased (Student's t-test (P < 0.05)). Also, increasing POM concentration resulted in increasing NLC particle size as noted in F3 (containing 20 mg POM) and F5 (containing 60 mg POM). The

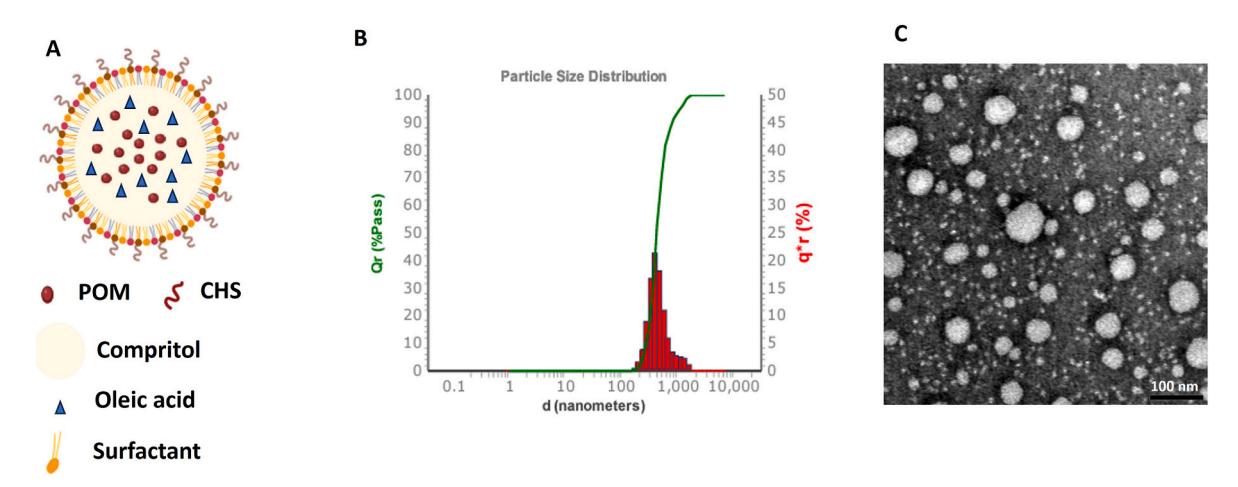


Fig. 3. (A) Schematic diagram of POM-CHS-NLCs, (B) Size distribution of F5 (selected formulation) and (C) TEM micrograph of F5 (selected formulation).

**Table 2**Composition, particle size, PDI, zeta potential and % EE of NLCs.

Formulation	POM	Oleic acid	CHS	Particle size (nm)	PDI	Zeta potential (mV)	% EE
F1	_	35 mg	_	$64.7 \pm 0.34$	$0.315\pm0.03$	$-17\pm1.34$	_
F2	20 mg			$163.9\pm1.2$	$0.274\pm0.08$	$-20\pm0.89$	$93.34 \pm 0.67$
F3	20 mg		0.5 %	$273.9 \pm 0.98$	$0.156\pm0.06$	$-24\pm0.45$	$96.34 \pm 0.34$
F4	_			$106.8\pm1.12$	$0.350\pm0.12$	$-21\pm0.78$	_
F5	60 mg			$341\pm2.5$	$0.281\pm0.04$	$-30\pm0.98$	$98.89 \pm 0.12$

particle size of the former was 273.9  $\pm$  0.98 nm meanwhile the particle size of the latter was 341  $\pm$  2.5 nm. These findings are along with the results previously reported by Zewail et al. [18].

As Table 2 demonstrates that the PDI of different formulations was less than 0.4, indicating that different NLCs formulations were homogenously dispersed [13].

High zeta potential has a substantial influence on the stability of nanocarriers. High surface charges provide repulsive forces that hinder particle coalescence and aggregation [40]. The increase in the negative surface charge upon encapsulation of POM may be attributed to the negative surface charge of POM [58]. Zeta potential increased from  $-17\pm1.34$  mV (F1) to  $-20\pm0.89$  mV (F2). Also, increasing POM concentration from 20 g (F3) to 60 mg (F5) increased zeta potential value from  $-24\pm0.45$  mV to  $-30\pm0.98$  mV, respectively. Furthermore, coating NLCs with CHS resulted in increasing zeta potential value. Zeta potential increased from  $-20\pm0.89$  mV to  $-24\pm0.45$  mV in F2 (uncoated NLCs) and F3 (CHS-coated NLCs). These findings are in agreement with the results previously reported by Zewail et al., who noted that coating leflunomide-loaded NLCs with CHS resulted in increasing their negative surface charge [18].

# 4.4. EE %

As depicted in Table 2, different formulations had high EE %. The high values of POM EE % suggest that the NLCs' lipid composition is suitable for POM entrapment [18]. This is along with previous reports of high EE% of poorly soluble drugs in NLCs [17,18]. This might be attributed to the imperfect inner architecture of NLCs, allowing improved accommodation of lipophilic medicines [59]. F4 had the highest EE %. Increasing POM concentration from 20 mg in F3 to 60 mg in F5 resulted in increasing EE % from 96.34  $\pm$  0.34 to 98.89  $\pm$  0.12 %, respectively. This coincides with previous reports [18]. F4 was selected for further characterization and its particle size distribution is elucidated in Fig. 3 B.

#### 4.5. TEM

As Fig. 3C demonstrates, F5 particles had a spherical uniform shape. There was no apparent clustering or aggregation. CHS coating layer was noted with a darker color in comparison with the NLCs core part. This findings coincides with the results previously reported by Zewail for the preparation of CHS coated leflunomide loaded NLCs [16,18].

#### 4.6. Characterization of F127 thermo-sensitive hydrogels

#### 4.6.1. Gelation temperature, pH, viscosity and injection time

Injectable sol-gel systems for biomedical applications have recently gained appeal as a potential alternative to implantable systems that need surgical insertion [60]. Upon thermosensitive hydrogels injection into the right place in the body, they transition from a sol to a gel at 37  $^{\circ}\text{C}$ , serving as a gel depot for extended drug release. The absence of organic solvents, cross-linkers, and externally applied triggers provides significant advantages over chemically cross linked hydrogels [35]. Injectable thermosensitive hydrogels can function as reservoirs that can be introduced into particularly targeted locations in the body, including the

joints, as drug-loaded liquids before going through a first-order transition, resulting in flexible soft hydrogel matrices in situ at physiological temperature [61].

Pluronic (also known as Poloxamer) is an amphiphilic copolymer composed of hydrophilic polyethylene glycol and hydrophobic polypropylene oxide. It is a typical thermo-sensitive hydrogel that may resist sol-gel transition when temperature increases due to partial dehydration of polyethene glycol chains [29,62]. Pluronics are popular for their safety, bio adhesiveness, stability, and capability to develop gels at low concentrations at the body's temperature [61]. Their thermosensitive hydrogels have numerous applications in RA management [16,30,34].

Gelation time is an essential characteristic of hydrogels. To avert medication leaking from the injection site, gelation must transpire promptly following administration [34,63]. Based on our previous study we selected F127 concentration to be 20 w/v % as induces gelation at 37 °C of suitable time with no gelation at RT [30]. As demonstrated in Table 3, loading plain F127 hydrogels with free POM, F4 and F5 resulted in a significant (Student t-test (p < 0.05)) decrease in gelation time in comparison with plain gel. On the other hand, no significant changes were noted in the gelation time of F127 loaded with F4 (blank CHS-NLCs) and F5 (POM-CHS-NLCs).

Regarding pH hydrogels loaded with free POM or POM-CHS-NLCs (F5) showed a significant decrease in hydrogel pH and that may be ascribed to the acidic nature of POM [64]. Also, it can be noted that loading F127 with free POM and CHS-NLCs increased the viscosity of the corresponding hydrogels and consequently their injection time increased. Injection times of plain F127, F127 loaded with free POM, F4 and F5 were  $4\pm1.34, 6\pm1.23, 9\pm1.14$  and  $11\pm1.98$  s (Table 3). The increase in F127 viscosity and injection time upon incorporation of nanocarriers is in agreement with previous reports and may be ascribed to hydrophobic and ionic interactions between the nanocarriers and the gel matrix [16,30]. Zewail et al. reported the increase in the viscosity of F127 hydrogels upon loading with leflunomide-loaded CHS-coated NLCs [16]. Also, Farzaneh et al. even reported the increase in the viscosity of pluronic hydrogels upon loading with magnetic nanoparticles [65].

## 4.6.2. In vitro drug release

*In-vitro* drug release tests from nanoformulations are important to predict their *in-vivo* performance [66]. An *in vitro* release test was conducted for POM suspension, F5, free POM in F127 hydrogel, and F5 in F127 hydrogel. Fig. 4 demonstrates that POM suspension was completely released after 24 h, while F5 showed a biphasic sustained release pattern for 6 days with an initial burst effect of 15 % after 30 min (Fig. 4 insert). NLCs have a biphasic release characteristic, bursting

**Table 3**Thermo-gelling properties of plain F127 hydrogels and F 127 hydrogels loaded with free POM and POM-CHS-NLCs.

Hydrogel formulation	Gelation time at 37 °c (sec)	pН	Viscosity (cp)	Injection time (sec)
Plain F127 Free POM in F127	$55 \pm 1.13 \\ 48 \pm 0.67$	$7.23 \pm 0.02 \\ 6.89 \pm 0.16$	$\begin{array}{c} 210 \pm 0.34 \\ 220 \pm 0.76 \end{array}$	$\begin{array}{c} 4\pm1.34 \\ 6\pm1.23 \end{array}$
F4 in F127 F5 in F127	$\begin{array}{c} 37\pm0.45\\ 35\pm0.56 \end{array}$	$\begin{aligned} 7.18 &\pm 0.05 \\ 6.80 &\pm 0.22 \end{aligned}$	$\begin{array}{c} 240 \pm 1.45 \\ 243 \pm 1.89 \end{array}$	$\begin{array}{c}9\pm1.14\\11\pm1.98\end{array}$

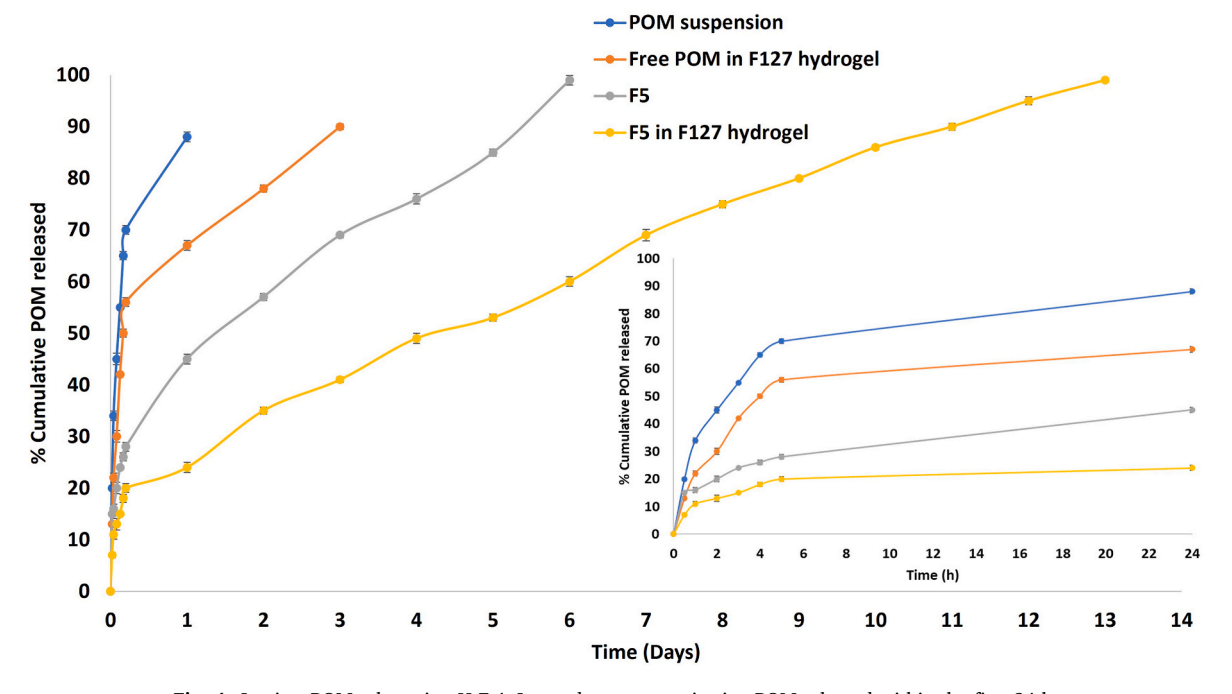


Fig. 4. In-vitro POM release in pH 7.4. Insert demonstrates in vitro POM released within the first 24 h.

immediately and then remaining constant. The liquid lipid located in the outer layers of the NLCs causes drug-enriched packing, leading to burst drug release at first by diffusion or matrix erosion via lipolysis. Then, the solid core lipid discharge medicines are continuously used after this [67].

A significant decrease in burst effect was noted in free POM and F5 upon loading in F127 hydrogels (Fig. 4 insert). Loading free POM and F5 in F127 hydrogels extended their release time from 24 h to 4 days for free POM and from 6 days to 13 days in F5. The effect of F127 hydrogel in retarding drug release and reducing burst effect may be ascribed to the decrease in the quantity and size of water channels within the

micellar structure of poloxamer would enhance hydrogel viscosity and regulate the release rate of the diffusing drug from the hydrogel matrix. [16,68]. The extended drug release from this dual nanoparticle-hydrogel system is primarily regulated by two processes. The medication diffuses first through the NLCs core and then into the hydrogel matrix. The second step involves the degradation or erosion of the hydrogel network [69].

## 4.7. Ex vivo insertion study of Ho-MNs

MNs were selected for injecting POM nanohybrid hydrogels as they

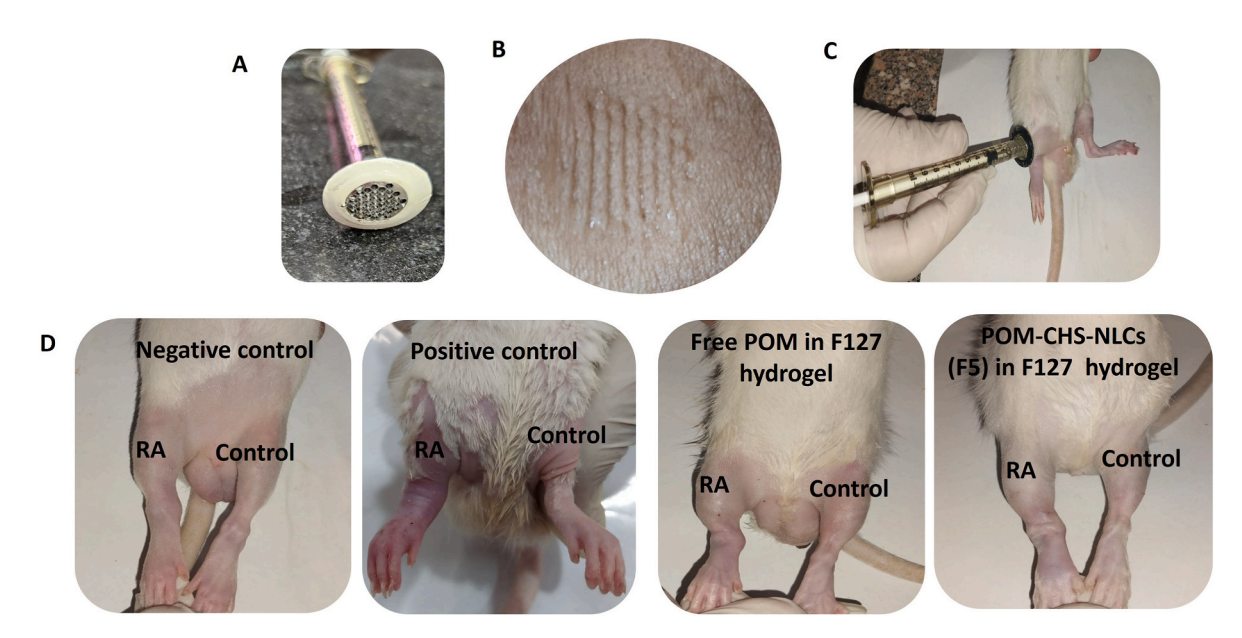


Fig. 5. A) AdminPen<sup>TM</sup> hollow MNs with 43 medical-grade stainless steel (SS316L) MN shafts of 1200 μm in height.Outer Diameter of Each MN: Approx. 200–250 μm (per manufacturer communication), Array Diameter: 1.3 cm circular array, Sterility: Electron beam (E-beam) sterilized by the manufacture. B) Image captured by a standard mobile camera (Samsung Galaxy S23 ultra, 12 MP, dual pixel) showing excised full-thickness human skin after insertion of MNs. (C) Intradermal administration of drug formulations using AdminPen<sup>TM</sup> hollow MNs into the arthritic joint in rats with AIA. (D) Shape of joints of different experimental groups at the end of the experimental period.

have the following advantages: ease of treatment termination, application of high localised drug orientation, painless self-administration, overcoming needle phobia, effective intradermal and transdermal drug availability, and suitability for sustained and controlled drug delivery. Therefore, MNs have the potential to enhance RA therapy outcomes as well as patient compliance [13].

The minimally invasive AdminPen<sup>TM</sup> Ho-MNs arrays (Fig. 5A) are engineered for intradermal or transdermal administration of liquid dispersions, as specified in US Patent No. 7,658,728 [70]. This circular MN array (diameter = 1.3 cm) features a novel design including 43 sharp-edged MN shafts, each measuring 1200  $\mu$ m in height and possessing an off-centred hollow pore on its side, therefore preventing needle blockage and facilitating efficient, continuous drug delivery. Microholes approximately 1100–1200  $\mu$ m deep are formed in both the stratum corneum and epidermal layers with the application of the AdminPen<sup>TM</sup> device [71,72]. Shortly after the extraction of microneedles, the created micropores collapse, and the skin barrier is promptly restored, mitigating any potential danger of skin infection. Considering the aforementioned advantages, AdminPen<sup>TM</sup> Ho-MNs were meticulously selected to effectively administer the designed POM-NLCs through the skin layers.

The AdminPen<sup>TM</sup> array used in this study is a ready-made stainless steel MN array that can be used to inject liquid medications for transdermal and intradermal delivery. Since they are made from stainless steel, no stability studies are required. Also, the sterility of AdminPen<sup>TM</sup> was guaranteed by the manufacturer [23].

The efficacy of MNs is contingent upon their insertion efficiency, as the stratum corneum must be effectively penetrated for the MN array to achieve its intended impact. Effective skin penetration with AdminPen^TM Ho-MNs is essential for the successful transdermal distribution of POM-NLCs. Excised dermal specimens and Parafilm M@ membranes serve as skin models to evaluate the penetration efficacy of microneedles.

In our previous work [13,37,72], we conducted **histological** and **visual confirmation** of microneedle penetration using excised human skin and Parafilm M® membrane models. These studies demonstrated that the AdminPen<sup>TM</sup> Ho-MNs achieved consistent penetration, with a **measured average depth of 889 \mum in Parafilm M®**, which is over **80**% **of the needle length**. Additionally, we validated the **effective skin penetration** in these studies, which directly supports the findings in our current research.

Moreover, a previous study by the author Abd-El-Azim [23] demonstrated that the currently used AdminPen<sup>TM</sup> Ho-MNs could be successfully inserted through Parafilm M® membrane, achieving a penetration depth of 889  $\mu m$ , which is greater than 80 % of the needle's real height. Also pore closure kinetics by AdminPen<sup>TM</sup> Ho-MNs was investigated by Abd El Azim and was monitored by recording OCT images every 2 min for the porcine skin after removal of AdminPen<sup>TM</sup> Ho-MNs. The healing process was started after 2-4 min, and complete restoration of skin barrier properties was noted after 10 min [23]. Literature indicates that excised human skin has been established as the "gold standard" in in-vitro testing [73,74]. In this study excised human skin was utilized to assess the insertion capabilities of the AdminPen<sup>TM</sup> Ho-MNs. AdminPen<sup>TM</sup> Ho-MNs liquid injection device should be mounted on any available standard syringe pre-filled with the liquid formulation, and inserted manually into the skin using both the thumb and the index finger by applying a force equivalent to that used to press a stamp onto an envelope for 30 s [72,75]. The force exerted by the human thumb for MNs insertion was previously proven to be equivalent to manual skin application force using human thumb pressure, as previously shown by Larrañeta et al. [76]. Furthermore, sterility of AdminPen<sup>TM</sup> was guaranteed by the manufacturer [72].

The images presented in Fig. 5 B demonstrate complete insertion, resulting in 43 dermal micropores corresponding to the 43 MNs in the array, with distinct interspaces evident, resulting in 100 % penetration. The results demonstrated effective skin penetrat and highlighted the

robust mechanical strength of the employed MNs. The anticipated MN-nanohybrid hydrogel combined delivery approach presents a promising potential for the effective treatment of RA.

#### 4.8. In vivo study

RA was successfully induced in mice and rats using a variety of techniques, including AIA, which is efficacious in inducing RA-associated physiological alterations [77]. Prior research has proven the efficiency of this induction paradigm in causing RA, as evidenced by histological inspection of the positive control dissected joints and the determination of numerous inflammatory mediators [30,39,78].

Arthritis medication typically necessitates long-term use, and conventional methods such as oral delivery or injections can lead to gastrointestinal side effects and present challenges for patients over extended periods. Recent advancements in MN technology have facilitated novel approaches to transdermal delivery of arthritis medications, owing to its benefits of painless skin penetration and effective localized administration [1]. The transdermal route offers several advantages such as bypassing hepatic first-pass metabolism, minimizing off-target adverse effects, and providing a rapid onset of action [13].

RA treatment was started at day 4 of the experiment and the whole experiment was conducted for 14 days. Treatments were administered as two 200  $\mu$ l doses at day 4 and day 9. Doses were administered using AdminPen<sup>TM</sup> Ho-MNs array in the right knee joints.

#### 4.8.1. Joint diameter assessment

Joint diameters were evaluated at days 0, 4, 7 and 14 as illustrated in Fig. 6. All groups except the negative control showed swelling and increased joint diameter on day 4. The group treated with POM-CHS-NLCs in F127 hydrogel demonstrated a more rapid reduction in joint diameter at day 7 compared with the group treated with free POM in F127 hydrogel. At day 14 the group treated with POM-CHS-NLCs in F127 hydrogel had comparable joint diameters to the negative control. This was further confirmed by the morphology of the joints of different experimental groups (Fig. 5D).

# 4.8.2. ELISA

Cytokines are powerful immunoregulatory factors that may play a direct role in chronic rheumatic illnesses' dysregulated immune systems. Interleukin-1b (IL-1b), Interleukin-2 (IL-2), and TNF- $\alpha$  have all been linked to the development of RA as mediators of chronic inflammation. Serum levels of IL-1b and TNF- $\alpha$ , as measured by radioimmunoassay, were significantly elevated in patients with RA compared to healthy controls matched for sex and age [79].

The rapid cell division associated with the inflammatory response in RA leads to a hypoxic environment in the synovium and increased intra- articular pressure. This leads to recurrent cycles of hypoxia and reoxygenation, increasing the production of reactive oxygen species (ROS) via cellular oxidative phosphorylation. This may activate transcription factors such as NF- $\kappa$ B and hypoxia-inducible factor-1 $\alpha$  (HIF-1 $\alpha$ ), which are responsive to oxygen levels. This will lead to a spectrum of gene expression that perpetuates synovitis. The activation of the ROS-induced NF- $\kappa$ B pathway may imply the increased production of IL-1 and TNF- $\alpha$ , establishing a positive feedback loop in the self-activation of proinflammatory cytokines [80].

Lipid peroxidation's main aldehyde consequence is MDA, a 3-carbon dialdehyde that enzymes can metabolize or react with proteins and tissues to form biomolecular damage. Many reactive electrophile species, including MDA, cause toxic stress in cells. Antioxidant therapy may offer new complementary RA-disease therapeutic alternatives 49].

Also, MMP-3 has a pivotal role in the pathology of RA. Elevated serum levels of MMP-3 have been observed in patients with RA compared to those with osteoarthritis, and these levels are associated with the progression of structural damage in RA patients [81].

On day 14, blood samples were collected and serum levels of TNF- $\alpha$ ,

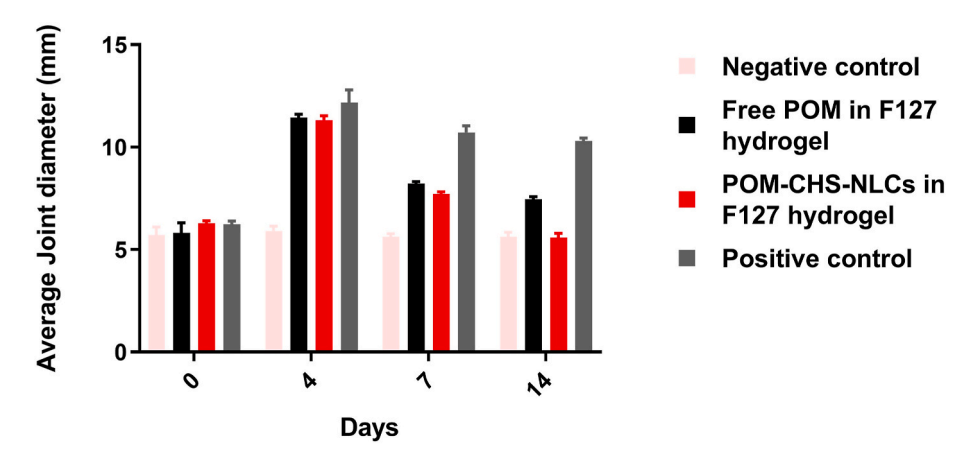


Fig. 6. Average joint diameter measurements in different experimental groups at day 0, 4, 7 and 14.

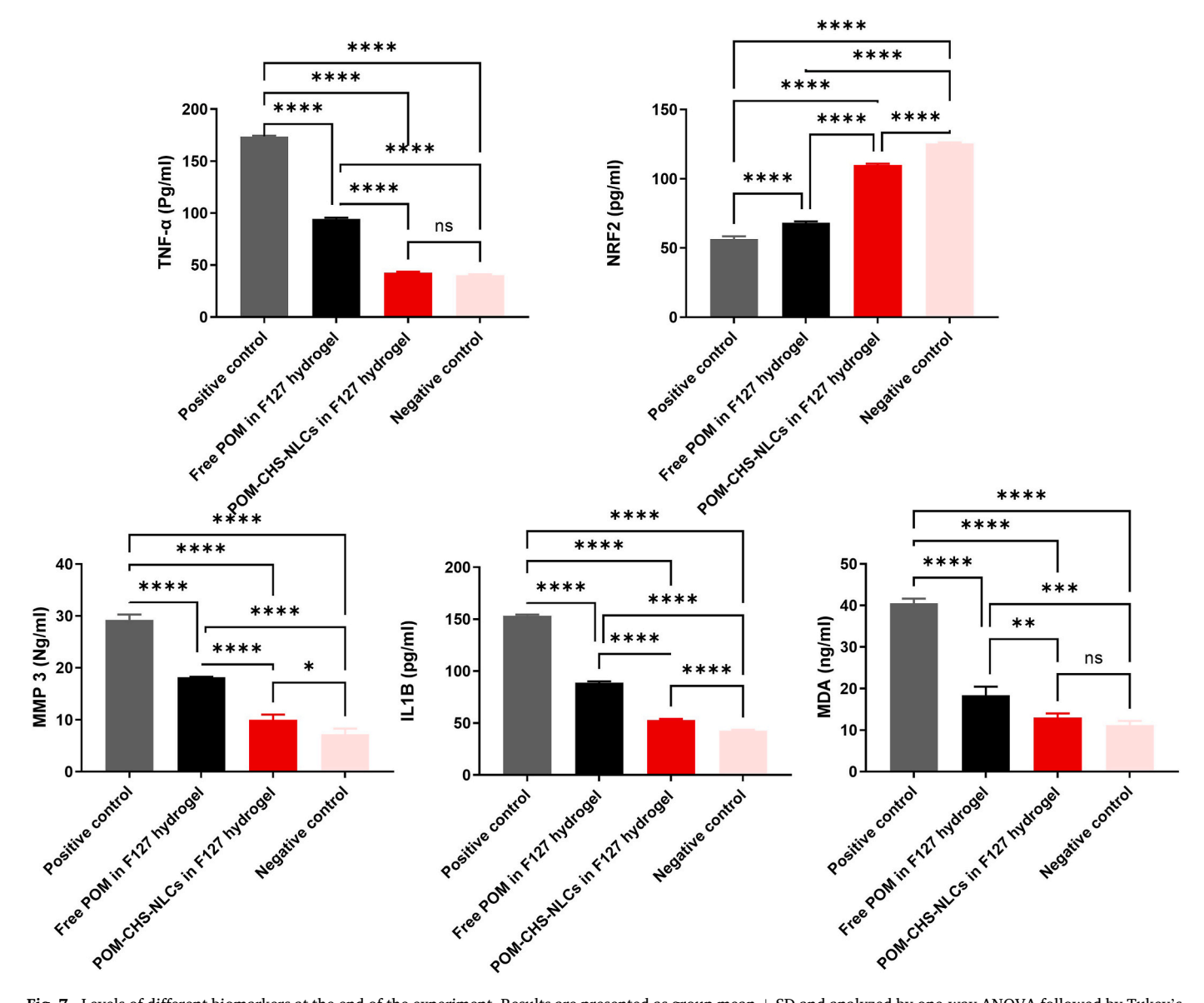


Fig. 7. Levels of different biomarkers at the end of the experiment. Results are presented as group mean  $\pm$  SD and analyzed by one-way ANOVA followed by Tukey's test. , \*\*p < 0.01, \*\*\*p < 0.001, and \*\*\*\*p < 0.0001.

Web version of this article.)

#### IL-1, MDA, NRF2 and MMP3 were evaluated (Fig. 7).

Levels of MDA and TNF- $\alpha$  were comparable to the negative control with no statistically significant differences (One way ANOVA p < 0.0001). Tugcu et al. previously reported the ability of POM to reduce MDA levels [82]. Also, Du et al. reported that punicalagin and ellagic acid which are the main components in POM exert their anti-inflammatory effect through blocking lipopolysaccharide induced phosphorylation, degradation of IkB, and nuclear translocation of p65 [83].

TNF- $\alpha$  levels were 173.5, 94.4, 42.6 and 40 pg/ml in the positive control, groups treated with free POM, POM-CHS-NLCs in F127 hydrogel and the negative control, respectively. This agrees with the previously reported results on the ability of POM to reduce TNF- $\alpha$  levels [83, 84]. Also, levels of IL-1 increased by 3.6, 2 and 1.2 folds in the positive control, groups treated with F127 hydrogels loaded with free POM and POM-CHS-NLCs, respectively in comparison to the negative control. This is along with previous reports [85,86].

Moreover, levels of MMP3 were 29.2, 18.2, 10 and 7.2 Ng/ml in the

#### **Negative control**

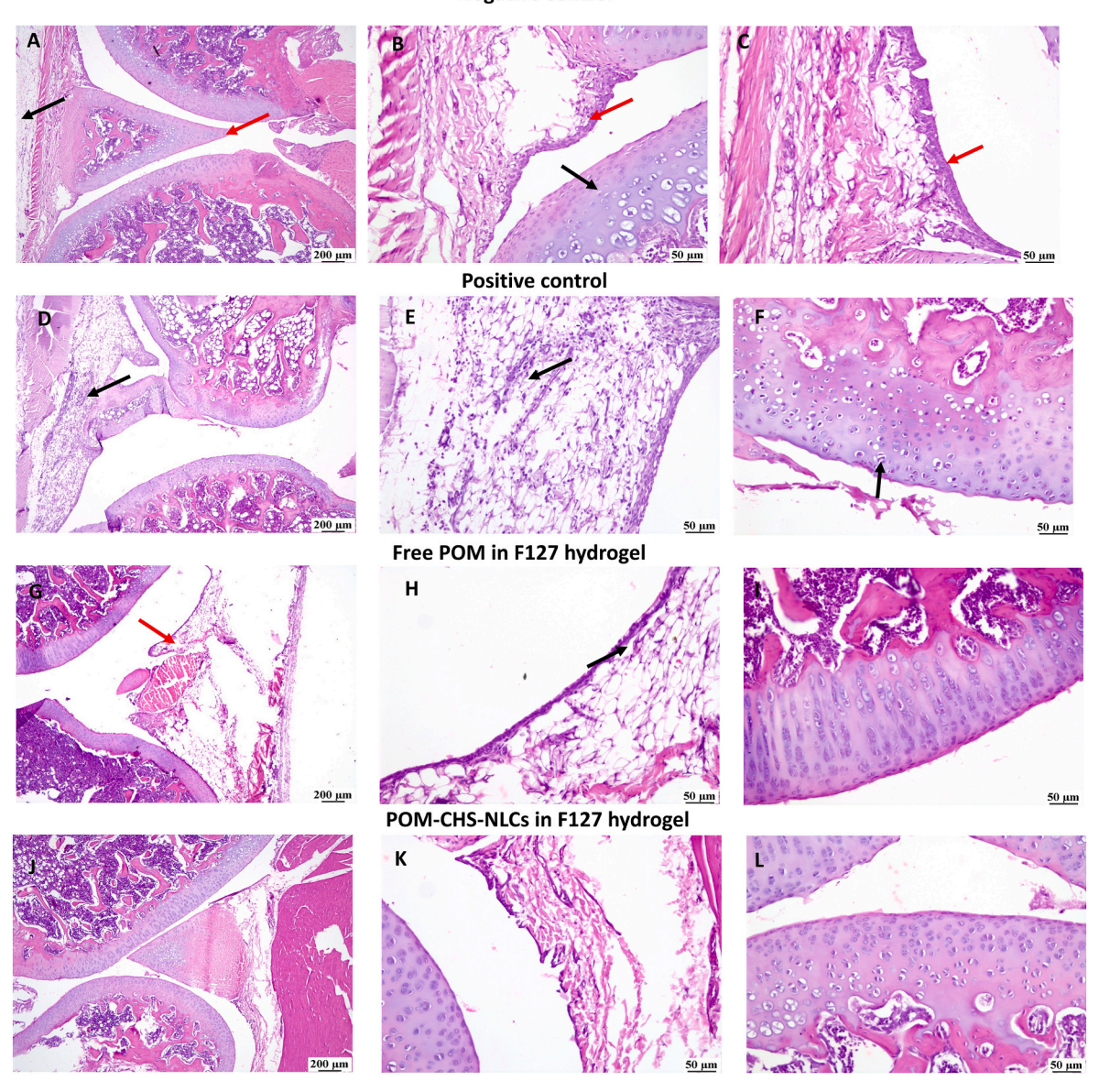


Fig. 8. Histopathological examination of dissected joints. A) Photomicrograph of joint, negative control group showing normal joint (red arrow) and subcutaneous tissue (black arrow) (H&E). B) Photomicrograph of joint, negative control group higher magnification showing normal joint including synovial membrane (red arrow) and articular cartilage (black arrow) (H&E). C) Photomicrograph of joint, negative control group higher magnification showing normal joint including synovial membrane (red arrow) (H&E). D) Photomicrograph of joint, positive control group showing arthritis extending into the joint capsule (arrow) (H&E). E) Photomicrograph of joint, positive control group higher magnification showing inflammatory cells infiltration extending into the joint capsule (arrow) (H&E). F) Photomicrograph of joint, positive control group higher magnification showing degeneration in some chondrocytes in the articular cartilage (black arrow) (H&E). G) Photomicrograph of joint, Free POM in F127 hydrogel group showing fewer inflammatory cells infiltration in the joint capsule (red arrow) (H&E). H) Photomicrograph of joint, Free POM in F127 hydrogel group higher magnification showing apparently normal articular cartilage (H&E). J) Photomicrograph of joint, Free POM in F127 hydrogel group higher magnification showing apparently normal articular cartilage (H&E). J) Photomicrograph of joint, POM-CHS-NLCs in F127 hydrogel group higher magnification showing apparently normal articular cartilage (H&E). J) Photomicrograph of joint, POM-CHS-NLCs in F127 hydrogel group higher magnification showing apparently normal articular cartilage (H&E). J) Photomicrograph of joint, POM-CHS-NLCs in F127 hydrogel group higher magnification showing apparently normal articular cartilage (H&E). J) Photomicrograph of joint, POM-CHS-NLCs in F127 hydrogel group higher magnification showing apparently normal articular cartilage (H&E).

fication showing apparently normal articular cartilage and synovial membrane (H&E). L) Photomicrograph of joint, POM-CHS-NLCs in F127 hydrogel group higher magnification showing apparently normal articular cartilage (H&E). (For interpretation of the references to color in this figure legend, the reader is referred to the

positive control, groups treated with free POM, POM-CHS-NLCs in F127 hydrogel and the negative control, respectively. The anti-inflammatory effects of POM may be attributed to the ability of POM phytochemicals to decrease the expression levels of extracellular-signal-regulated kinase (ERK), Jun N-terminal kinase (JNK), and p38–mitogen-activated protein kinase (p38 MAPK) [83].

Preclinical studies on PPE have demonstrated promising results in various animal models of arthritis disease. For example, studies involving rats with induced arthritis have shown that PPE significantly reduced joint swelling, pain, and inflammation through inhibition of the activation of nuclear factor kappa B (NF- $\kappa$ B) and this would lower the levels of pro-inflammatory cytokines (such as TNF- $\alpha$ , IL-1 $\beta$ , and IL-6) and enzymes (like COX-2 and MMPs) [44,87]. A recent clinical trial showed that supplementation with PPE reduced serum inflammatory markers, including hs-CRP, NF- $\kappa$ B, MCP-1, and MMP-1, in women with knee osteoarthritis. These findings suggest that PPE supplementation could be beneficial as a comprehensive strategy to manage inflammation in women suffering from knee osteoarthritis [88].

Also, aprevious research demonstrated that pomegranate juice, extract, and the isolated bioactive compounds delphinidin and penicillin decreased factor nuclear factor- $\kappa B$  (NF- $\kappa B$ ) activation in various cell types. The study revealed that pomegranate inhibited the expression of IL-6, IL-8, and NF- $\kappa B$  target genes in intestinal cells exposed to proinflammatory stimuli [89].

Furthermore, levels of NRF2 decreased by 2.2, 1.8, and 1.1 folds in the positive control, groups treated with F127 hydrogels loaded with free POM and POM-CHS-NLCs, respectively compared with the negative control group. These findings confirm POMs' antioxidant capacity that occurs through various mechanisms, including reducing the rate of lipid peroxidation, scavenging or destroying ROS, triggering or preventing multiple signalling pathways, and regulating how genes are expressed [90].

#### 4.8.3. Histopathological examination of dissected joints

Microscopic examination of the joint from the negative control group (Fig. 8A–C) revealed the normal histologic structure of the joint. Fig. 8 A illustrates normal joint (red arrow) and subcutaneous tissue (black arrow). Higher magnifications in Fig. 8 B and C illustrated the normal joint structure including synovial membrane (red arrow) and articular cartilage (black arrow).

On the contrary, the positive group (Fig. 8D–F) showed intense periarticular inflammatory cell infiltration extending into the joint capsule. The synovial lining showed sloughing and degeneration.). Higher magnification in Fig. 8 F demonstrated degeneration in some chondrocytes in the articular cartilage (black arrow).

Free POM in F127 hydrogel (Fig. 8G–I) showed moderate improvement, as the examined sections revealed fewer inflammatory cell infiltrations into the joint capsule (red arrow Fig. 8 G). Higher magnification in Fig. 8H and I showed mild inflammation in the joint capsule (arrow). Both synovial lining and articular cartilage were normal. Previous histological analysis in osteoarthritis by Shivnath et al. has revealed that PPE extract can preserve cartilage integrity and reduce synovial membrane inflammation [91].

On the other hand, the group treated with POM-CHS-NLCs in F127 (Fig. 8J-L) showed normal joints, including the joint capsule, synovial lining, and articular cartilage.

The anti-inflammatory properties of POM appear to be associated with its phenolic compounds, including punicalagin, ellagic acid, and anthocyanins. Furthermore, the fatty acids found in pomegranate seeds have been shown to exhibit significant anti-inflammatory properties [44–46,92].

The POM extract can decrease cytokine levels, reduce joint swelling and suppress joint destruction due to the primary impact of the POM extract to decrease oxidative stress, suppress the p38-MAPK pathway, and inhibit the activation of the transcription NF- $\kappa$ B. The activation of p38-MAPK and NF- $\kappa$ B is closely linked to an elevated gene expression of

TNF- $\alpha$ , IL-1 $\beta$ , monocyte chemoattractant protein-1 (MCP1), inducible nitric oxide synthase (NOS), and cyclo-oxygenase-2, which are essential mediators of joint inflammation and the pathogenesis of RA [5].

The superior effect of POM-CHS-NLCs over free POM may be ascribed to the impact of nanotechnology in improving the bioavailability and bioactivity of phytomedicine by reducing particle size to nanoparticles, altering surface properties, and increasing aqueous solubility and permeability through biological membranes [93]. In addition to the innate joint healing properties that would provide synergistic effects in joint healing [18]. Also, Ho-MNs used in injecting POM-loaded F127 hydrogels ensured effective local delivery of POM that would be further extended as a result of incorporation of POM and POM-CHS-NLCs in F127 hydrogels.

#### 5. Conclusion

POM-loaded NLCs were successfully prepared using the melt emulsification technique. The optimized formulation was loaded in F127 thermosensitive hydrogel to prepare nanohybrid hydrogels. Nanohybrid hydrogels extended the POM release period for 13 days in comparison to POM NLCs (6 days). In vivo results in rats with AIA RA model have proven the ability of POM to suppress RA progression and promote joint healing and highlighted the superiority of POM NLCs in F127 hydrogel over free POM in F127 hydrogel elucidating the role of nanoencapsulation in improving the solubility and the pharmacological activity of POM. In addition, F127 hydrogel served as a depot that could extend the POM release period and hence sustain its pharmacological effects reducing its administration frequency. Moreover, AdminPenTM Ho-MNs ensured deep penetration of the prepared formulations in a minimally invasive manner that may aid in improving patient compliance and assuring treatment effectiveness. Overall, combining nanohybrid thermosensitive hydrogel with MNs seems to be an effective patient friendly approach to improve RA treatment outcomes. The effectiveness of MN treatment for RA can justify its cost by offering superior outcomes compared to traditional treatments. By delivering medication directly into the affected areas, MNs enhance drug absorption, leading to quicker symptom relief and potentially reducing the overall amount of medication needed. This targeted approach minimizes side effects and decreases the likelihood of relapse, which can lower long-term healthcare expenses. Additionally, improved patient adherence and fewer required treatments can offset the initial investment, making MN therapy a cost-effective option in the long run.

# CRediT authorship contribution statement

Mariam Zewail: Writing – original draft, Validation, Methodology, Data curation. Haidy Abbas: Writing – review & editing, Validation, Supervision, Resources, Methodology. Nesrine El Sayed: Validation, Supervision, Software, Project administration, Conceptualization. Nihal M. El Newehy: Writing – review & editing, Writing – original draft, Software, Methodology, Investigation, Data curation. Heba Abd-El-Azim: Validation, Supervision, Methodology, Investigation, Data curation, Conceptualization.

#### Declaration of competing interest

The authors declare that they have no known competing financial interests or personal relationships that could have appeared to influence the work reported in this paper.

## Data availability

No data was used for the research described in the article.

#### References

- [1] J. Wang, et al., Promising strategies for transdermal delivery of arthritis drugs: microneedle systems, Pharmaceutics 14 (8) (2022) 1736.
- [2] V.D. Bui, et al., Chondroitin sulfate-based microneedles for transdermal delivery of stem cell-derived extracellular vesicles to treat rheumatoid arthritis, J. Contr. Release 375 (2024) 105–115.
- [3] R.J. Black, et al., Global, regional, and national burden of rheumatoid arthritis, 1990–2020, and projections to 2050: a systematic analysis of the global burden of disease study 2021, The Lancet Rheumatology 5 (10) (2023) e594–e610.
- [4] C.S. Lau, Burden of rheumatoid arthritis and forecasted prevalence to 2050, The Lancet Rheumatology 5 (10) (2023) e567–e568.
- [5] M. Shukla, et al., Consumption of hydrolyzable tannins-rich pomegranate extract suppresses inflammation and joint damage in rheumatoid arthritis, Nutrition 24 (7–8) (2008) 733–743.
- [6] Q. Wang, et al., Nanomedicines for the treatment of rheumatoid arthritis: state of art and potential therapeutic strategies, Acta Pharm. Sin. B 11 (5) (2021) 1158–1174.
- [7] C. Recio, I. Andujar, J.L. Rios, Anti-inflammatory agents from plants: progress and potential. Curr. Med. Chem. 19 (14) (2012) 2088–2103
- [8] S. Ge, et al., A unique understanding of traditional medicine of pomegranate, Punica granatum L. and its current research status, J. Ethnopharmacol. 271 (2021) 113877.
- [9] J. Bekir, et al., Assessment of antioxidant, anti-inflammatory, anti-cholinesterase and cytotoxic activities of pomegranate (Punica granatum) leaves, Food Chem. Toxicol. 55 (2013) 470–475.
- [10] S. Noreen, et al., Phytochemicals and pharmacology of pomegranate (Punica granatum L.): nutraceutical benefits and industrial applications: a review, Front. Nutr. 12 (2025) 1528897.
- [11] Q. Xiang, et al., The bioactivity and applications of pomegranate peel extract: a review, J. Food Biochem. 46 (7) (2022) e14105.
- [12] H.A. El-Nashar, et al., Neuroprotective effect of artichoke-based nanoformulation in sporadic alzheimer's disease mouse model: focus on antioxidant, antiinflammatory, and amyloidogenic pathways, Pharmaceuticals 15 (10) (2022) 1202
- [13] H. Abd-El-Azim, et al., Non-invasive management of rheumatoid arthritis using hollow microneedles as a tool for transdermal delivery of teriflunomide loaded solid lipid nanoparticles, Int. J. Pharm. (2023) 123334.
- [14] S.N.A. Syed Azhar, et al., Nanostructured lipid carriers-hydrogels system for drug delivery: nanohybrid technology perspective, Molecules 27 (1) (2022) 289.
- [15] A. Rani, et al., Nanostructured lipid carriers (NLC)-based topical formulation of hesperidin for effective treatment of psoriasis, Pharmaceutics 17 (4) (2025) 478.
- [16] M. Zewail, et al., Synergistic and receptor-mediated targeting of arthritic joints via intra-articular injectable smart hydrogels containing leflunomide-loaded lipid nanocarriers, Drug Delivery and Translational Research 11 (6) (2021) 2496–2519.
- [17] M. Zewail, et al., Hyaluronic acid coated teriflunomide (A771726) loaded lipid carriers for the oral management of rheumatoid arthritis, Int. J. Pharm. 623 (2022) 121939.
- [18] M. Zewail, et al., Coated nanostructured lipid carriers targeting the Joints-An effective and safe approach for the oral management of rheumatoid arthritis, Int. J. Pharm. 567 (2019) 118447.
- [19] S. Khan, A. Sharma, V. Jain, An overview of nanostructured lipid carriers and its application in drug delivery through different routes, Adv. Pharmaceut. Bull. 13 (3) (2022) 446.
- [20] J. Wen, et al., Intra-articular nanoparticles based therapies for osteoarthritis and rheumatoid arthritis management, Mater. Today Bio 19 (2023) 100597.
- [21] B. Siddiqui, et al., Folate decorated chitosan-chondroitin sulfate nanoparticles loaded hydrogel for targeting macrophages against rheumatoid arthritis, Carbohydr. Polym. 327 (2024) 121683.
- [22] S. Karmarkar, et al., Navigating rheumatoid arthritis: insights into ligand-anchored nanoparticle strategies for anti-inflammatory therapy and relief, RSC Pharmaceutics 2 (1) (2025) 19–43.
- [23] H. Abd-El-Azim, et al., Hollow microneedle assisted intradermal delivery of hypericin lipid nanocapsules with light enabled photodynamic therapy against skin cancer, J. Contr. Release 348 (2022) 849–869.
- [24] N.M. El Newehy, et al., Comparative metabolomics reveal intraspecies variability in bioactive compounds of different cultivars of pomegranate fruit (Punica granatum L.) and their waste by-products, J. Sci. Food Agric. 102 (13) (2022) 5891–5902.
- [25] M. Kokabi, S.N. Ebrahimi, Polyphenol enriched extract of pomegranate peel; a novel precursor for the biosynthesis of zinc oxide nanoparticles and application in sunscreens, Pharm. Sci. 27 (1) (2020) 102–110.
- [26] G.I. Sakellari, et al., Formulation design, production and characterisation of solid lipid nanoparticles (SLN) and nanostructured lipid carriers (NLC) for the encapsulation of a model hydrophobic active, Food hydrocolloids for health 1 (2021) 100024.
- [27] F. Rahman, E. Hendradi, T. Purwanti, Lipids selection and methods of nanostructured lipid carrier for topical use, International Journal of Drug Delivery Technology 14 (3) (2024) 1880–1889.
- [28] S. Padhi, R. Mazumder, S. Bisht, Preformulation screening of lipids using solubility parameter concept in conjunction with experimental research to develop ceftriaxone loaded nanostructured lipid carriers, Brazilian Journal of Pharmaceutical Sciences 59 (2023) e21308.
- [29] A. Lupu, et al., Temperature sensitive pluronic F127-Based gels incorporating natural therapeutic agents, Macromol. Mater. Eng. 310 (4) (2025) 2400341.

- [30] S. Makled, et al., Melatonin hyalurosomes in collagen thermosensitive gel as a potential repurposing approach for rheumatoid arthritis management via the intraarticular route, Int. J. Pharm. (2024) 124449.
- [31] M.A. El-Nabarawi, et al., Dapsone-loaded invasomes as a potential treatment of acne: preparation, characterization, and in vivo skin deposition assay, AAPS PharmSciTech 19 (2018) 2174–2184.
- [32] Y.B. Schuetz, R. Gurny, O. Jordan, A novel thermoresponsive hydrogel based on chitosan, Eur. J. Pharm. Biopharm. 68 (1) (2008) 19–25.
- [33] Q.S. Zhao, et al., Effect of organic and inorganic acids on chitosan/ glycerophosphate thermosensitive hydrogel, J. Sol. Gel Sci. Technol. 50 (1) (2009) 111–118.
- [34] M. Zewail, N. Nafee, N. Boraie, Intra-articular dual drug delivery for synergistic rheumatoid arthritis treatment, J. Pharmaceut. Sci. 110 (7) (2021) 2808–2822.
- [35] N. Nafee, M. Zewail, N. Boraie, Alendronate-loaded, biodegradable smart hydrogel: a promising injectable depot formulation for osteoporosis, J. Drug Target. 26 (7) (2018) 563–575.
- [36] N. Badawi, et al., Development of pomegranate extract-loaded solid lipid nanoparticles: quality by design approach to screen the variables affecting the quality attributes and characterization, ACS Omega 5 (34) (2020) 21712–21721.
- [37] M. Zewail, et al., Combined photodynamic therapy and hollow microneedle approach for effective non-invasive delivery of hypericin for the management of imiquimod-induced psoriasis, J. Drug Target. (2024) 1–28 (just-accepted).
- [38] H. Abd-El-Azim, et al., Hypericin emulsomes combined with hollow microneedles as a non-invasive photodynamic platform for rheumatoid arthritis treatment, Int. J. Pharm. (2024) 123876.
- [39] H. Abbas, et al., Development and evaluation of novel leflunomide SPION bioemulsomes for the intra-articular treatment of arthritis, Pharmaceutics 14 (10) (2022) 2005.
- [40] H. Abbas, N.M. El-Deeb, M. Zewail, PLA-Coated imwitor® 900 K-based herbal colloidal carriers as novel candidates for the intra-articular treatment of arthritis, Pharmaceut. Dev. Technol. 26 (6) (2021) 682–692.
- [41] R.K. Gautam, et al., Rosmarinic acid attenuates inflammation in experimentally induced arthritis in wistar rats, using Freund's complete adjuvant, International journal of rheumatic diseases 22 (7) (2019) 1247–1254.
- [42] M.H. Boskabady, et al., Pharmacological effects of Rosa damascena, Iranian journal of basic medical sciences 14 (4) (2011) 295.
- [43] C.F.A. Culling, Handbook of Histopathological and Histochemical Techniques: including Museum Techniques, Butterworth-Heinemann, 2013.
- [44] R. Karwasra, et al., Pomegranate supplementation attenuates inflammation, joint dysfunction via inhibition of NF-κB signaling pathway in experimental models of rheumatoid arthritis, J. Food Biochem. 43 (8) (2019) e12959.
- [45] M.A. Khan, et al., Ellagic acid protects type II collagen induced arthritis in rat via diminution of IKB phosphorylation and suppression IKB-NF-kB complex activation: in vivo and in silico study, Inflammopharmacology 30 (5) (2022) 1729–1743.
- [46] C.-J. Lee, et al., Inhibitory effects of punicalagin from Punica granatum against type II collagenase-induced osteoarthritis, J. Funct.Foods 41 (2018) 216–222.
- [47] V. Stefanou, et al., Anti-inflammatory properties of pomegranate, Int. J. Adv. Res. Microbiol. Immunol 2 (1) (2020) 1–13.
- [48] F. Liu, et al., Simultaneous quantitative analysis and in vitro anti-arthritic effects of five polyphenols from Terminalia chebula, Front. Physiol. 14 (2023) 1138947.
- [49] R. Makkar, et al., Investigating the anti-arthritic potential of gallic acid from Tecoma stans leaves via phytosome based formulation and examining physical, hematological effects, and molecular dynamics simulations, J. Biol. Regul. Homeost. Agents 38 (4) (2024) 3177–3187.
- [50] V. Parisi, et al., Comparative chemical analysis of eight Punica granatum L. peel cultivars and their antioxidant and anti-inflammatory activities, Antioxidants 11 (11) (2022) 2262.
- [51] A.M. El-Moghazy, et al., Chemical constituents of ornamental pomegranate and its antioxidant and anti-inflammatory activities in comparison with edible pomegranate, J. Pharmacogn. Phytochem. 5 (4) (2016) 88–94.
- [52] Y. Soleimanian, et al., Propolis wax nanostructured lipid carrier for delivery of  $\beta$  sitosterol: effect of formulation variables on physicochemical properties, Food Chem. 260 (2018) 97–105.
- [53] M. Zewail, et al., Combined photodynamic therapy and hollow microneedle approach for effective non-invasive delivery of hypericin for the management of imiquimod-induced psoriasis, J. Drug Target. 32 (8) (2024) 941–952.
- [54] C. Santa-María, et al., Update on anti-inflammatory molecular mechanisms induced by oleic acid, Nutrients 15 (1) (2023) 224.
- [55] T. Venkatesh, et al., Nanosuspensions: ideal approach for the drug delivery of poorly water soluble drugs, Pharm. Lett. 3 (2) (2011) 203–213.
- [56] Y. Soleimanian, et al., Formulation and characterization of novel nanostructured lipid carriers made from beeswax, propolis wax and pomegranate seed oil, Food Chem. 244 (2018) 83–92.
- [57] M. Zewail, Leflunomide nanocarriers: a new prospect of therapeutic applications, J. Microencapsul. 41 (8) (2024) 715–738.
- [58] J. Zareei, et al., Investigation of the potential of pomegranate peel as a treatment option for heavy metal contaminated wastewater: experimental and modeling approaches, Heliyon 10 (14) (2024) e34619.
- [59] A.C. Ortiz, et al., Development of a nanostructured lipid carrier (NLC) by a low-energy method, comparison of release kinetics and molecular dynamics simulation, Pharmaceutics 13 (4) (2021) 531.
- [60] S. Gordon, et al., In vitro and in vivo investigation of thermosensitive chitosan hydrogels containing silica nanoparticles for vaccine delivery, Eur. J. Pharmaceut. Sci. 41 (2) (2010) 360–368.

- [61] B. Shriky, et al., Pluronic F127 thermosensitive injectable smart hydrogels for controlled drug delivery system development, J. Colloid Interface Sci. 565 (2020) 119–130.
- [62] C.T. Huynh, M.K. Nguyen, D.S. Lee, Injectable block copolymer hydrogels: achievements and future challenges for biomedical applications, Macromolecules 44 (17) (2011) 6629–6636.
- [63] S. Lii, M. Liu, B. Ni, An injectable oxidized carboxymethylcellulose/N-succinylchitosan hydrogel system for protein delivery, CHEM ENG J 160 (2) (2010) 779–787
- [64] S. Papanov, E. Petkova, I. Ivanov, Polyphenols content and antioxidant activity of various pomegranate juices, Bulg. Chem. Commun. 51 (2019) 113–116.
- [65] M. Farzaneh, S.A. Hassanzadeh-Tabrizi, N. Mokhtarian, Preparation of an injectable thermosensitive pluronic F127/γ-Fe2O3 hydrogel for combined hyperthermia and localized drug delivery for cancer treatment, Polym. Adv. Technol. 35 (11) (2024) e6616.
- [66] D. Solomon, et al., Role of in vitro release methods in liposomal formulation development: challenges and regulatory perspective, AAPS J. 19 (2017) 1669–1681
- [67] V.N. Thuy, et al., Nanostructured lipid carriers and their potential applications for versatile drug delivery via oral administration, OpenNano 8 (2022) 100064.
- [68] N.A.H.A. Youssef, et al., A novel nasal almotriptan loaded solid lipid nanoparticles in mucoadhesive in situ gel formulation for brain targeting: preparation, characterization and in vivo evaluation, Int. J. Pharm. 548 (1) (2018) 609–624.
- [69] X. Li, et al., A novel composite drug delivery system: honokiol nanoparticles in thermosensitive hydrogel based on chitosan, J. Nanosci. Nanotechnol. 9 (8) (2009) 4586-4592
- [70] V.V. Yuzhakov, in: Microneedle Array, Patch, and Applicator for Transdermal Drug Delivery, 2010. https://patents.google.com/patent/WO2007081430A3/en.
- [71] V.V. Yuzhakov, The AdminPen<sup>TM</sup> microneedle device for painless & convenient drug delivery, Drug Delivery Technology 10 (4) (2010) 32–36.
- [72] H. Abd-El-Azim, et al., Hollow microneedle assisted intradermal delivery of hypericin lipid nanocapsules with light enabled photodynamic therapy against skin cancer, J. Contr. Release: Official Journal of the Controlled Release Society (2022) 849–869.
- [73] E. Abd, et al., Skin models for the testing of transdermal drugs, J. Clin. Pharmacol. 8 (2016) 163.
- [74] M. Zewail, et al., Intradermal delivery of teriflunomide loaded emulsomes using hollow microneedles for effective minimally invasive psoriasis management, Eur. J. Pharm. Biopharm. (2025) 114692.
- [75] V.V. Yuzhakov, The AdminPen™ microneedle device for painless & convenient drug delivery, Drug Deliv. Technol 10 (4) (2010) 32–36.
- [76] E. Larrañeta, et al., A proposed model membrane and test method for microneedle insertion studies, Int. J. Pharm. 472 (1–2) (2014) 65–73.
- [77] N. Choudhary, L.K. Bhatt, K.S. Prabhavalkar, Experimental animal models for rheumatoid arthritis, Immunopharmacol. Immunotoxicol. 40 (3) (2018) 193–200.

- [78] M. Zewail, et al., Innovative rheumatoid arthritis management using injection replacement approach via dual therapeutic effects of hyalurosomes-encapsulated luteolin and dexamethasone, Colloids Surf. B Biointerfaces (2025) 114497.
- [79] L. Altomonte, et al., Serum levels of interleukin-1b, tumour necrosis factor-a and interleukin-2 in rheumatoid arthritis. Correlation with disease activity, Clin. Rheumatol. 11 (1992) 202–205.
- [80] G.A. Nabih, et al., Serum malondialdehyde as a marker of oxidative stress in rheumatoid arthritis, Egyptian Rheumatology and Rehabilitation 51 (1) (2024) 43.
- [81] S. Sun, et al., The active form of MMP-3 is a marker of synovial inflammation and cartilage turnover in inflammatory joint diseases, BMC Muscoskelet. Disord. 15 (2014) 1–8.
- [82] B. Tugcu, et al., Protective effect of pomegranate juice on retinal oxidative stress in streptozotocin-induced diabetic rats, Int. J. Ophthalmol. 10 (11) (2017) 1662.
- [83] L. Du, et al., Pomegranate peel polyphenols inhibits inflammation in LPS-Induced RAW264. 7 macrophages via the suppression of TLR4/NF-κB pathway activation, Food Nutr. Res. 63 (2019).
- [84] G. Pepe, et al., Bioactive polyphenols from pomegranate juice reduce 5-fluorouracil-induced intestinal mucositis in intestinal epithelial cells, Antioxidants 9 (8) (2020) 699.
- [85] F. Mastrogiovanni, et al., Antioxidant and anti-inflammatory effects of pomegranate peel extracts on bovine mammary epithelial cells BME-UV1, Nat. Prod. Res. 34 (10) (2020) 1465–1469.
- [86] K. Ren, R. Torres, Role of interleukin-1 $\beta$  during pain and inflammation, Brain Res. Rev. 60 (1) (2009) 57–64.
- [87] D. Wahyuningsih, et al., The prophylactic effects of pomegranate peel in a rat model of rheumatoid arthritis: study on arthritis score and expression of inflammatory, Markers 10 (1) (2020) 57–66.
- [88] M. Rafraf, et al., Effects of pomegranate (Punica granatum L.) peel extract supplementation on markers of inflammation and serum matrix metalloproteinase 1 in women with knee osteoarthritis: a randomized double-blind placebocontrolled study, Nutr. Metab. Insights 17 (2024) 11786388241243266.
- [89] H.M. Shaheen, A.A. Alsenosy, Nuclear factor kappa B inhibition as a therapeutic target of nutraceuticals in arthritis, osteoarthritis, and related inflammation, in: Bioactive Food as Dietary Interventions for Arthritis and Related Inflammatory Diseases, Elsevier, 2019, pp. 437–453.
- [90] A. Lavoro, et al., Pomegranate: a promising avenue against the Most common chronic diseases and their associated risk factors, International Journal of Functional Nutrition 2 (2) (2021) 1–12.
- [91] N. Shivnath, et al., Antiosteoarthritic effect of Punica granatum L. peel extract on collagenase induced osteoarthritis rat by modulation of COL-2, MMP-3, and COX-2 expression, Environ. Toxicol. 36 (1) (2021) 5–15.
- [92] A. Malek Mahdavi, N. Seyedsadjadi, Z. Javadivala, Potential effects of pomegranate (Punica granatum) on rheumatoid arthritis: a systematic review, Int. J. Clin. Pract. 75 (8) (2021) e13999.
- [93] X. Li, et al., Nanocarriers in the enhancement of therapeutic efficacy of natural drugs, BIO Integration 2 (2) (2021) 40–49.